UNCLASSIFIED

AD 427231

DEFENSE DOCUMENTATION CENTER

FOR

SCIENTIFIC AND TECHNICAL INFORMATION
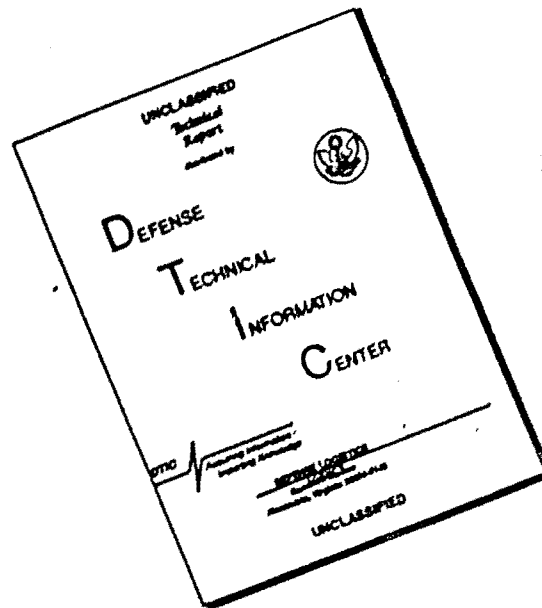
CAMERON STATION, ALEXANDRIA, VIRGINIA

UNCLASSIFIED

DISCLAIMER NOTICE

THIS DOCUMENT IS BEST QUALITY AVAILABLE. THE COPY FURNISHED TO DTIC CONTAINED A SIGNIFICANT NUMBER OF PAGES WHICH DO NOT REPRODUCE LEGIBLY.

64-7

RTD-TDR-63-4085

DEVELOPMENT OF AERODYNAMICALLY COMPENSATED PITOT-STATIC TUBES FOR USE ON THE XB-70 AIRCRAFT

TECHNICAL DOCUMENTARY REPORT No. RTD-TDR-63-4085

NOVEMBER 1963

DIRECTORATE OF CREW SUBSYSTEMS ENGINEERING
RESEARCH AND TECHNOLOGY DIVISION
AIR FORCE SYSTEMS COMMAND
WRIGHT-PATTERSON AIR FORCE BASE, OHIO

JAN 2 0 1964

Project No. 8201, Task No. 820112

NOTICES

When Government drawings, specifications, or other data are used for any purpose other than in connection with a definitely related Government procurement operation, the United States Government thereby incurs no responsibility nor any obligation whatsoever; and the fact that the Government may have formulated, furnished, or in any way supplied the said drawings, specifications, or other data, is not to be regarded by implication or otherwise as in any manner licensing the holder or any other person or corporation, or conveying any rights or permission to manufacture, use, or sell any patented invention that may in any way be related thereto.

Qualified requesters may obtain copies of this report from the Defense Documentation Center (DDC), (formerly ASTIA), Cameron Station, Bldg. 5, 5010 Duke Street, Alexandria 4, Virginia

This report has been released to the Office of Technical Services, U.S. Department of Commerce, Washington 25, D.C., in stock quantities for sale to the general public.

Copies of this report should not be returned to the Research and Technology Division unless return is required by security considerations, contractual obligations, or notice on a specific document.

FOREWORD

The research and development work, upon which this report is based, was accomplished by the Department of Aeronautical Research of the Rosemount Engineering Company, under USAF Contract Number AF 33(600)42658. The program was initiated by the Aeronautical Systems Division, Directorate of Operational Support Engineering,[*] under Project No. 8201, Task No. 820112. Task engineer was Lt. William Imfeld of the Flight Vehicle Division, Flight Control Branch.[**]

Acknowledgement is made for the assistance and advice of Mr. C. J. Jolley of the Flight Control Branch and for the assistance of the following project engineers of wind tunnel facilities used to test models developed under this contract: Mr. Virgil S. Ritchie of the NASA Full Scale Analysis Branch, Langley Field, Virginia; Mr. Lewis E. Rittenhouse, Mr. Warren E. White, and Mr. Terry A. Martin of the Propulsion Wind Tunnel Facility and Mr. Russel E. Brillhart, Jr. of the Von Karman Gas Dynamics Facility at the Arnold Engineering Development Center, Arnold Air Force Station, Tennessee.

The technical advice of Dr. Frank D. Werner of the Rosemount Engineering Company is also gratefully acknowledged as is the assistance of Mr. Willard L. Moline in supervision of model design and fabrication and Mr. Loren A. Lemmerman in calculations and preparing figures for the report.

ABSTRACT

Two types of aerodynamically compensated pitot-static tubes were investigated to find a design suitable for flight testing on the XB-70 aircraft. First configurations, contoured-nose type, utilized compensated subsonic static pressure ports located on the rear portion of an ogival nose and uncompensated supersonic static ports located aft on the cylindrical portion of the tube. A Mach switch is normally needed to switch from the subsonic port to the supersonic ports as sonic conditions are reached at the compensated static ports. However, a specific design was developed and tested which exhibited very small supersonic pressure errors at the compensated static ports located on the contoured-nose. Second configurations, contoured-afterbody type, used a gentle downward sloping curvature located immediately aft of the compensated static ports. The same static ports may be used for both subsonic and supersonic flight, eliminating the need for a Mach switch.

Both theoretical analysis and wind tunnel experiments were used to determine subsonic and supersonic performance of a number of models of each of the two types. The level of aerodynamic compensation, compatible with XB-70 pressure errors, was generally predicted with good accuracy using theoretical methods. Emperical results were used to determine the static pressure effect due to cutting off the tip of the contour-nose units to form a pitot opening and to determine angle of attack influences for the static ports on both types.
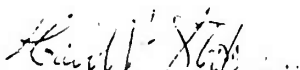
Two units of the contoured-afterbody type, designated REC Model 855D, were furnished to the Air Force for flight test evaluation on the XB-70.

PUBLICATION REVIEW

This report has been reviewed and is approved.

FOR THE COMMANDER:

DAVID V. STOCKMAN
Chief, Instrument Systems Division
Directorate of Crew Subsystems Engineering

TABLE OF CONTENTS

LIST OF TABLES

LIST OF APPENDICES

LIST OF ILLUSTRATIONS

LIST OF ILLUSTRATIONS (CONT)

LIST OF ILLUSTRATIONS (CONT.)

LIST OF ILLUSTRATIONS (CONT.)

SECTION 1

                                INTRODUCTION

     Subsonic, transonic and supersonic static and total pressure measurements are
usually obtained during aircraft flight by means of a pitot-static tube extending for-
ward of the aircraft's nose. The main advantage of this location is that supersonically
the pitot and static pressure sensing ports are ahead of the bow shock wave of the air-
craft and are isolated from the distribution of pressure around the aircraft. Sub-
sonically, however, the aircraft's flow field is propagated forward such that pressure
sensed at the static ports is greater than the true ambient value. The pressure
difference is usually called the position error and in order to arrive at true static
pressures it is necessary to apply a position correction. The position error can be
reduced by placing a body, an aerodynamic compensator, in the flow field such as to
induce a pressure correction approximately equal to and of opposite sign to the position
error induced by the fuselage. The aerodynamic compensator forms an integral part
of an aerodynamically compensated pitot-static tube and generally has the form of a
gently sloping contour before, aft, or around the static pressure port location.

     Two types of compensated pitot-static tubes have been investigated under this
contract The first type incorporates a design previously investigated by NASA,
Reference 1, and has subsonic static ports located on the rear portion of an ogive
nose of the tube. The forward tip of the ogive is eliminated to form a pitot opening.
The tube has two sets of static ports: a compensated set for subsonic flight and an
uncompensated set located back on the cylindrical portion of the tube for supersonic
flight A Mach switch is needed to switch from the subsonic set to the supersonic set
as sonic conditions are reached at the compensated static ports. The possibility of
using the forward set of ports for both subsonic and supersonic flight, thus eliminating
the need for a Mach switch, was also investigated.

     The second design investigated for application to the XB-70 Aircraft, REC Model
855D* uses a gentle downward sloping curvature located immediately aft of the static

* Patent Pending

pressure ports. The Model 855D utilizes only one set of static ports for both subsonic and supersonic flight. The subsonic pressure will be compensated but during super-sonic flight the compensating shape will be isolated from the static ports, thus giving no correction. With this design there is no need for a Mach switch.

Because the position correction needed for the XB-70 has not been determined by flight data, it has been estimated using analytical methods and available experimental data. The predicted values were then checked against wind tunnel data obtained for pressure distribution ahead of a scale model of the XB-70

The work developed under this contract was supported by the Directorate of Operational Support Engineering. Flight Vehicle Division, Flight Control Branch of the Aeronautical Systems Division.

SECTION 2

PREDICTION OF PRESSURE FIELD AHEAD OF AIRCRAFT

2.1. THEORETICAL PREDICTION.

The static pressure error ahead of the XB-70 was computed using both analytical and emperical relationships for zero degrees angle of attack. The error at low Mach numbers was determined as a function of distance ahead of the aircraft using the well known linearized slender-body theory, e.g., References 2 and 3. For this computation, equivalent cross sectional areas were determined for numerous fuselage stations over the first 40 feet of the fuselage. Two areas were obtained for each station, one above the centerline of the nose boom and the other below, and equivalent radii for each area were plotted as a function of distance aft of the fuselage-nose boom intersection. The mean slope of the fuselage and equivalent radii were then found for small intervals of Δx over the first 40 feet of fuselage. By placing these values in the subsonic slender-body theory differential equation and integrating numerically, the static pressure error as a function of distance ahead of the fuselage was found. The error for a true Mach number of 0.4 is shown on Figure 1. The canards and wing platform as well as the portion of fuselage beyond 40 feet from the nose of the XB-70 were not taken into account in the prediction shown on Figure 1 because their remoteness from the nose of the aircraft insures negligible effects on the pressure distribution ahead of the aircraft when compared with the influence of the forward portion of the fuselage.

A verification of the procedure used to compute the errors shown on Figure 1 was obtained by predicting the pressure distribution ahead of a slender-nose transonic aircraft model for which pressure distribution had been determined thru wind tunnel tests, Reference 1. Only the forward ogive section of the model, shown on Figure 10(a) of Reference 1, was used in the analysis. A comparison between pressure distribution computed from the exact nose shape of the model and the distribution found experimentally are shown on Figure 2A for $M_\infty = 0.4$. The two agree well within the probable absolute accuracy of the wind tunnel.

Use of slender-body theory for predicting position error was also established in an early report, Reference 4. Experimental results for pressure error ahead of various fuselage shapes were found to be in good agreement with slender body theory at low Mach number.

2.2. COMPRESSIBILITY INFLUENCE:

Because subsonic slender-body theory becomes invalid when local sonic flow conditions are reached on the surface of the fuselage, emperical relationships were used to extend the low subsonic error shown on Figure 1 to the Mach number at which the bow shock wave passes downstream of specific locations ahead of the aircraft. It has been established experimentally, Reference 4, that pressure error ahead of a slender body in terms of $\Delta P/q_c$, where q_c is compressible dynamic pressure, is essentially constant for true Mach numbers up to the point where local sonic flow is reached on the body. Using the constant $\Delta P/q_c$ assumption and experimental transonic results for pressure error ahead of the slender aircraft model of Reference 1, a ratio of pressure coefficients vs. Mach number was formulated. Results are shown on Figure 2(B) for two XB-70 nose boom lengths: The standard nose boom where the static ports of the pitot-static tube would be located approximately 3 feet ahead of the aircraft and the extended nose boom used on the first flight test aircraft where the static pressure ports would be located approximately 6 feet ahead of the aircraft. The emperical relationship shown on Figure 2(B) is presented as ratios of pressure coefficients using the experimental values at $M_\infty = 0.4$ as a base.

The computed values for pressure coefficient ahead of the aircraft at $M_\infty = 0.4$, Figure 1, and the emperical compressibility relationship, Figure 2(B), were used to compute static pressure error for a number of nose boom lengths which cover the area of interest for possible location of static ports. The REC estimated errors are shown on Figure 3 in terms of indicated compressible dynamic pressure as a function of indicated Mach number. An earlier estimate of pressure errors ahead of the XB-70, Figure 4, had been made by North American Aviation in their original Equipment Procurement Specification Report, No. NA5-76123. This estimate did

-4-

not take into account the exact shape of the aircraft's nose. Because there was a significant difference between the REC computed values, Figure 3, and those estimated by North American, Figure 4, the pressure errors estimated by REC are used in the remainder of this report. The REC prediction of pressure error is presented on Figure 5 in terms of $(P_i - P_\infty)/P_i$ as a function of indicated Mach number. Because indicated pressure and Mach number are the direct parameters measured in wind tunnels when testing compensated pitot-static tubes, all wind tunnel data presented in the following sections are shown in this parameter.

Each static pressure port location ahead of the aircraft will have a specific indicated Mach number and corresponding pressure error for which the bow shock wave passes downstream of the ports. At this value the position errors, $(P_i - P_\infty)/P_i$, will drop abruptly to zero and the indicated Mach number felt at the static ports will become true Mach number. The transition region is illustrated by dotted lines on Figure 5 Assuming negligible thickness of the bow shock wave, position errors and indicated Mach numbers in this transition region will not be felt at the static pressure ports. Indicated Mach number as a function of true Mach number for the REC estimate of position error is presented on Figure 6 for the same distance ahead of the aircraft shown on Figure 5.

2.3. WIND TUNNEL VERIFICATION.

Experimental pressure distribution ahead of a 1/36 scale model of the XB-70 Aircraft was obtained in the NASA 8-foot Transonic Wind Tunnel at Langley Field, Virginia. Data for two locations ahead of the aircraft, $x = 60.951$ inches and $x - 80.302$ inches. are shown on Figures 7A and 7B. Superimposed on these figures are REC predicted values for the same locations. There is very good agreement between the predicted pressure errors and experimental data.

Compensated static ports on the Model 855D, to be used on the first flight test aircraft, will be located at $x = 71.291$ inches ahead of the aircraft. Predicted static pressure error at this location, Figure 7C, agree very well with the average of the wind tunnel data given on Figures 7A and 7B. The exact distance, $x = 71.291$ inches, is approximately midway between the wind tunnel data locations, $(60.951 + 80.302)/2 = 70.627$ inches. Averaging the data should be a realistic approximation because the

pressure distribution, as shown on Figure 1, is nearly linear with x between these two locations.

SECTION 3

WIND TUNNEL TEST PROGRAM

3.1. WIND TUNNEL FACILITIES.

Five wind tunnel facilities were used to verify performance characteristics of compensated pitot-static tubes developed under this contract. General description for each of the wind tunnels are included in the following paragraphs.

3.1.1. Langley 8-Foot Transonic Tunnel.

The Langley 8-Foot Transonic Tunnel, located at the NASA Langley Research Center, Langley Field, Virginia, was used to obtain data for three pitot-static tube models over a Mach number range from 0.4 to 1.2. Detailed characteristics of the facility are given in Reference 5 and a general description is included in Reference 6. The tunnel has a 1/9-open slotted test section approximately 8 feet in diameter. During the test program the stagnation pressure was about 2120 lb/ft^2, the average tunnel total temperature was 120° F, and the Reynold's Number per foot varied from about 2.5×10^6 at M = 0.4 to 4×10^6 at M = 1.2. Altitude simulation ranged from approximately 3000 feet at M = 0.4 to 22,500 feet at M = 1.2.

Static pressure measurements were referenced to the pressure in the plenum chamber surrounding the test section. Because plenum pressures were nearly identical to the free-stream static pressures and pressure fluctuations in the test section were small, Reference 5, plenum pressure was assumed equal to free-stream static pressure and corrections for flow irregularities were not applied. Repeatability of measurements has been estimated, References 1 and 5, at $\Delta M \cong \pm 0.003$ subsonically and supersonically in shock-free flow. This corresponds to static pressure variations ranging from $\Delta P/P = \pm 0.0016$ at M = 0.4 to ± 0.0027 at M = 1.0. However, boundary-reflected disturbances could decrease supersonic accuracies to ΔM greater than ± 0.04 or values of $\Delta P/P$ near ± 0.005.

Pressure variations of $\Delta P/P = \pm 0.005$ represent pressure-altitude errors of approximately ± 100 feet in the stratosphere and indicates the approximate upper

limit of usefulness of subsonic wind tunnel data. The exact pressure-altitude errors assuming standard atmospheric conditions are shown on Figure 8A. A comparison chart, Figure 8B, gives the corresponding compressible pressure coefficient errors and Mach number errors as a function of Mach number for a constant static pressure error of $\Delta P/P = 0.005$.

3.1.2. Langley 4 x 4 Foot Supersonic Tunnel.

This wind tunnel is also located at the NASA Langley Research Center. A general description of the facility is included in Reference 6. The test section is 54 inches wide with fixed side walls, and the upper and lower walls are adjustable so that the height will vary from approximately 51 to 64 inches. Four pitot-static tube models were tested in the facility at a free stream Mach number of approximately 2.2. Total temperature was about 100° F. Two settings of stagnation pressure, P_o = 1058 lb/ft^2 and 720 lb/ft^2, were used for altitude simulation of 63,000 and 78,000 feet, respectively. Although a calibration check of the tunnel was made during the test period using a one inch diameter static pressure survey tube which extended into the nozzle of the tunnel, the accuracy of the data remained questionable. A new survey apparatus has been fabricated and a second check of the flow characteristics in the tunnel will be made. For this reason data obtained in the 4-foot supersonic tunnel has not been included in this report.

3.1.3. AEDC One Foot Transonic Model Tunnel.

The AEDC One Foot Transonic Model Tunnel, located at the Propulsion Wind Tunnel Facility of the Arnold Engineering Development Center, Tennessee, was used to obtain data for seven compensated pitot-static tube designs and two wind tunnel survey models over a Mach number range from 0.55 to 1.5. A detailed description of the facility and its operating parameters are given in References 7 and 8. Descriptions of tests run at this facility and presentation of the data obtained are reported in References 9 and 10.

The Transonic Model Tunnel is a continuous-flow, open-circuit wind tunnel. The test section is comprised of four perforated walls forming a test section 12 x 12 inches in cross section and 37.5 inches in length. The tunnel was operated at stagnation

pressures from 2800 to 2900 lb/ft^2 and the stagnation temperature varied from 125 to 200° F. Reynold's Number per foot ranged from 3.8 x 10^6 to 5.5 x 10^6. Simulated pressure altitude varied from about -2,100 feet at M = 0.55 to 24,800 feet at M = 1.5.

Pressure measurements were references to the pressure in the plenum chamber surrounding the test section. Because the plenum pressure varied considerably from the average free stream static pressure in the tunnel, calibration factors obtained from a static pressure centerline survey were used to relate the data obtained to free stream conditions. Two additional survey models were used to detect local flow irregularities at the exact test section location of static ports on the compensated pitot-static tubes tested. The cumulative error of flow variations, pressure measurements, and any random errors was estimated in Reference 9 and 10 at approximately $\Delta P/P = \pm 0.005$ subsonically. Significant wind-tunnel wall interference errors were present supersonically and consequently the cumulative static pressure errors were believed to generally exceed $\Delta P/P = \pm 0.005$ throughout the supersonic range.

3.1.4. <u>AEDC E-I Supersonic Wind Tunnel</u>.

The E-I tunnel, located at the Von Karman Gas Dynamics Facility, Arnold Engineering Development Center, Tennessee, is an intermittent supersonic wind tunnel with a 12" x 12" test section and a flexible plate nozzle. A detailed description of the facility is given in References 8 and 11. Five compensated pitot-static tube designs and two wind tunnel survey models were tested at Mach numbers of 1.45, 2.0, 2.5, 3.0, and 4.0. During the test program total temperature was in the range from 490° R to 540° R and stilling chamber total pressures were about 2260 psf. at M = 1.45, 1843.2 psf. at M = 2.0, 4050 psf. at M = 2.5, and 8640 psf. at M = 3.0 and M = 4.0. Corresponding altitude simulations are about 29,000 ft. at M = 1.45, and about 50,000 feet for M = 2.0, 2.5, and 3.0, and about 80,000 feet at M = 4.0. Reynold's number per inch was 0.4 x 10^6 at M = 1.45, 0.3 x 10^6 at M = 2.0, 0.5 x 10^6 at M = 2.5, 0.8 x 10^6 at M = 3.0, and .5 x 10^6 at M = 4.0.

The mean repeatability of data, including instrumentation calibration uncertainties, system accuracies, and random errors, was estimated in Reference 11 at

$\Delta M \cong \pm 0.002$. All static pressure measurements obtained for the models were referenced to a flush wall tap on the sidewall of the tunnel located upstream of the nose of the models. Survey models with static ports at the same tunnel locations as the static ports on the compensated pitot-static tube models were used to correct the pressure sensed at the flush wall tap to free stream values. Total accuracies of the measurements should therefore be less than $\Delta M = \pm 0.004$. This will result in static pressure errors of about $\Delta P/P = \pm 0.0044$ provided there is no reflected wall interference.

3.1.5. REC Transonic Wind Tunnel.

The Rosemount Engineering Company transonic wind tunnel has a 3.6 inch by 17 inch test section that is 27 inches long. It utilizes local atmospheric conditions for total temperature and total pressure. The facility is described in detail in Reference 12. Although the REC tunnel is too small to obtain accurate measurements of absolute values of pressure compensation provided by a full scale compensated pitot-static tube, useful results were obtained for sensitivity to angle of attack of various static port locations and for the effect of placing a pitot opening on contoured nose design compensated pitot-static tubes. Data was obtained using a pressure difference method whereby differential pressures were measured with respect to pressure sensed at a flush wall tap located in the test section at a position remote from the model tested. By taking the differences in (static port pressure minus flush tap pressure) as the shape of the tube or location of the static ports are modified slightly, reliable data was obtained.

Data obtained was in the Mach number range from 0.3 to 0.7. Accuracy of individual static pressure measurements is within about ± 0.2 lb/ft^2. A limited amount of re-run data obtained for tests run at $M = 0.5$ utilizing the pressure differential technique indicated repeatability accuracy within $\Delta P/P = \pm 0.0005$.

3.2. WIND TUNNEL MODELS.

Thirteen wind tunnel models were fabricated and tested to verify performance characteristics of the two types of compensated pitot-static tubes developed for the XB-70 Aircraft. Four of the models incorporated the contoured-nose method of

aerodynamic compensation. They are designated in this report as the Type C Models. Seven of the models tested used the contoured-afterbody method of compensation and are referred to as the Type D Models. The remaining two models were survey models used to determine flow characteristics of the AEDC transonic and supersonic wind tunnel facilities.

3.2.1. Type C Wind Tunnel Models.

Dimensions and details of the four contoured-nose wind tunnel models are shown on Figure 9. Mounting dimensions represent those needed for connection to the nose boom of the XB-70 and were the same for all four models. A number of other dimensions including the overall length and pitot opening configuration were also common for the four models. Dimensions which varied are labeled A thru G and specific values for these dimensions on each model are given in tabular form on Figure 9. Nose coordinates for the models are also listed in tabular form. The coordinate "Y" is the radius of the nose at a distance "X" aft of the pitot opening.

The subsonic compensated static ports are referred to as the S_1 ports and are located on the contoured-nose portion of the Type C models. The angular location of the static ports, Dimensions F and G on Figure 9, were varied to obtain optimum subsonic and supersonic angle of attack performance. Two interconnected sets of supersonic static ports, designated S_2 ports, are located on the center portion of the Type C Models. On three of the models they were placed on a slight 0.5 degree taper. The S_2 ports are uncompensated subsonically, but give a true indication of static pressure supersonically. Because of the large supersonic errors normally present at the S_1 ports, a Mach switch would be needed to switch from the compensated S_1 ports to the supersonic S_2 ports as sonic conditions are reached. However, in this report, suitable design of the S_1 ports to provide true supersonic static pressure while retaining a desired level of subsonic compensation is also discussed. A third set of static ports, the S_3 ports, was placed on Model C-98. They sensed essentially the same pressures as the S_2 ports and would be used as a reference pressure for flight test evaluation.

-11-

3.2.2. Type D Wind Tunnel Models.

External configurations for the seven contoured-afterbody models are given on Figure 10. Mounting dimensions for the Type D models were identical to those used on the Type C models. Each of the "D" models had an overall length of 17.685 inches. The pitot nose configuration was identical for all seven models. A single set of static ports, designated S_1/S_2 ports, was used for both subsonic and supersonic flight. They are located on a slight taper which extends forward to the pitot nose. The compensating afterbody contour starts 0.062 inches aft of the S_1/S_2 ports. Coordinates of the contours used for the various models are given on Figure 10 in terms of radius "Y" of the tube as a function of distance "X" aft of the centerline through the S_1/S_2 ports. Subsonic compensation at the S_1/S_2 ports is achieved by the negative pressure induced by the contoured afterbody. Supersonically, the pressure effects of the afterbody contours are isolated from the S_1/S_2 ports enabling them to sense true static pressure.

On five of the models a second set of static ports, S_3 ports, was located one inch ahead of the S_1/S_2 ports. The S_3 ports are relatively remote from the afterbody contour and were designed to sense the indicated, or uncompensated, static pressure ahead of the aircraft subsonically and true static pressure supersonically. The S_3 ports will be used as a reference for flight test evaluation. Angular displacement of the S_1/S_2 ports and S_3 ports, dimensions G and H on Figure 10, were varied to obtain optimum subsonic and supersonic angle of attack performance.

3.2.3. Wind Tunnel Survey Models.

Dimensions for the two survey models used in the test program are shown on Figure 11. The short survey model, Model S-104, had the same overall length, pitot nose configuration, and rear adapter dimensions as the Type D models. Location of the S_2 ports on the S-104 correspond to the S_1/S_2 port location on all the Type D models with the exception of Model D-40 which had its S_1/S_2 ports located at the S_3 location on Model S-104. The short survey model was used primarily to determine the pressure effects of the pitot nose and rear adapter section on the Type D models.

The long survey model, Model S-139, had four sets of static ports. Location of the S_1 set corresponds to the S_1 ports on Model C-134. The S_2 and S_3 locations

correspond to the S_3 and S_1/S_2 port locations, respectively, on all the type D models with the exception of those on Model D-40. The rear S_4 ports on Survey Model S-139 are in the same position as the midpoint of the supersonic S_2 ports on the Type C models. The nose cone of the Model S-139 was extended far upstream of the static ports to eliminate any pressure effects of the nose. The long survey model was used to calibrate static pressure in both the transonic and supersonic tunnels at AEDC at the exact static port location on the Type C and D Models.

Wind tunnel adapters used in the various facilities incorporated the forward mounting dimensions of the XB-70 nose boom. The forward portion of the adapters is shown on Figure 11. Three different adapters used in the test program; one each for the Langley 8-Foot Transonic Tunnel, the Langley 4-Foot Supersonic Tunnel. and the AEDC Transonic and Supersonic Tunnels. The 1.872 inch maximum diameter was maintained for each, but the length of the adapters was varied to place static ports on the various models near the angle-of-attack center of rotation of the tunnels.

3.2.4. Dimensional Accuracies of Wind Tunnel Models.

Static pressure repeatability of compensated pitot-static tubes require extremely close machining tolerances, especially in the vicinity of the static pressure ports. All wind tunnel models tested were carefully checked to assure conformity to all the design dimensions specified for the models. Because of the immediate proximity of the compensating contours on the Type C and D Models to the compensating static ports, dimensional deviations of the contours from their designed shapes were closely measured and pressure errors caused by any deviations were analyzed. Results of the analysis are shown on Figure 12 for the Type C Models and on Figure 13 for the Type D Models. Because of the difficulty in accurately measuring the curvature of the compensating contours, an optical comparator was used and some of the tubes were rechecked one or more times to obtain reliable measurements. The approximate repeatability accuracy of measurements was ± 0.0005 inches. Deviation of actual radii from design radii for the compensating contours are shown on Figures 12(A) and 13(A). Using linearized small-perturbation theory, these deviations were used to compute the

-13-

approximate static pressure errors induced by the dimensional variations. The pressure errors are shown on Figures 12(B) and 13(B). For the majority of the models the computed static pressure errors were less than ± 0.002 which is well within the absolute accuracy of wind tunnel data.

3.3. WIND TUNNEL RESULTS FOR SURVEY MODELS S-104 AND S-139.

3.3.1. Subsonic Performance of Survey Models.

Survey Models S-104 and S-139 were used to locate secondary flow irregularities in the AEDC One Foot Transonic Model Tunnel at the exact tunnel locations of static ports on the various Type "C" and "D" compensated pitot-static tubes. They were also used to check the accuracy of determining absolute magnitude of free stream static pressure in the tunnel. As mentioned in the general description of the tunnel, Section 3.1.3, static pressure measurements were referenced to pressure in the plenum chamber surrounding the test section. Because plenum pressure varied considerably from the average free stream static pressure. calibration factors obtained from centerline surveys were used to relate the data obtained to free stream conditions. A simple calibration factor at each Mach number was used to cover the test section length in which the pressure ports of the test models were located. Secondary pressures fluctuation from the calibrated value at particular locations of static ports were not taken into account in data reduction. Examples of centerline surveys conducted in the tunnel and a description of the survey apparatus used are given in Reference 7.

Two series of tests were run in the tunnel. Because the test section was modified slightly between tests, different calibration factors were used in determining free stream conditions for the two tests. The short survey tube, Model S-104, was used to check calibration of the first test series. Results are shown on Figures 14(A) and 14(B). Data obtained for the long survey tube, Model S-139, run during the second test series, is shown on Figures 15(A) and 15(B). Because of the limiting size of the tunnel, reflected disturbances in the tunnel produced erratic and erroneous data at the supersonic test Mach numbers of 1.05, 1.1, 1.2 and 1.5. For this reason supersonic data has not been shown on Figures 14 and 15.

-14-

Over the subsonic Mach number range pressure influences of both the nose and rear adapter sections on the survey models are felt at the static ports. The pitot nose of Model S-104 or the nose cone on Model S-139 will induce a negative pressure effect at the static ports and the aft taper on the models together with the wind tunnel adapter will induce a positive pressure effect. As the port location is moved aft on the models, the nose effect will decrease and the rear taper and adapter effect will become more dominant resulting in a net increase in static pressure as the ports are moved aft. Data on Figure 14(A) for the short survey model shows the sensed pressure, P_s, at the three port locations was less than free stream pressure, P_i, indicating a predominance of nose effect. There is a fair amount of data scatter and the expected increasing pressure effect with increasing distance from the pitot nose is not demonstrated. Data for the long survey model, Figure 15(A), obtained during the second test series and using a different tunnel calibration does show an increase in pressure with decreasing distance to the aft taper, i.e., from the S_1 ports to the S_4 ports. The pressure difference, $(P_s - P_i)/P_i$, at corresponding port locations, S_2 ports on S-104 and S_3 ports on S-139. is also more positive for Model S-139 which is to be expected because of the extended nose cone on Model S-139. Pressure differences at the S_3 ports on Model S-139 agrees well with the calculated influence of the rear taper and wind tunnel adapter as will be discussed in Section 5.1. However, the negative influence of the pitot nose on Model S-104 was not believed to be as large as indicated by Figure 14(A). Although pressure influence of the pitot nose cannot be calculated accurately. based on previous wind tunnel data, compiled in Reference 13, it is believed that the pressure felt at all the static port locations on both models should be slightly positive compared to free stream static pressure, i.e., the influence of the nose will be smaller than the influence of the rear taper and wind tunnel adapter. Deviations from this assumption for the three static port locations on Model S-104, Figure 14(A). and the S_1 port location on Model S-139, Figure 15(A), could therefore be secondary calibration factors to be applied to data taken for the types "C" and "D" pitot-static tube models tested. However, because of uncertainty in the absolute magnitude of the correction. due primarily to limitations in accuracies of the wind tunnel data, and

-15-

because the deviations are not large, corrections were not applied to data shown in this report for the type C and D models.

Angle of attack performance of static ports on survey models S-104 and S-139 are shown on Figures 14(B) and 15(B), respectively. Static ports on the long survey model S-139 exhibited no large deviations with angles of attack. However, ports on the short survey model showed a definite decrease in sensed pressure with increasing angle of attack. Because the static ports on both models are placed at the angular location of ± 36°, their angle of attack trends should be identical. The negative pressure trend for ports on S-104 could be due to closeness of the pitot nose, although random deviations between data at the three distances from the nose, i.e., locations of the S_1, S_2, and S_3 ports. indicate that data accuracy limitations form a sizable portion of the angle of attack variation.

3.3.2. Supersonic Performance of Survey Models.

The long wind tunnel survey tube, Model S-139, was used to find the true static pressure level for the test series run in the AEDC E-I Supersonic Wind Tunnel. As shown on Figure 11, the Model S-139 nose was moved far upstream, 12.8 diameters from the closest set of static ports, to eliminate nose interference at the static ports. Supersonic data for Model S-139 is given on Figure 16. The data is presented in terms of $(P_s - P_w)/P_w$ where P_s is pressure sensed by the static ports and P_w is the pressure sensed by a flush wind tunnel wall tap. For the survey model P_s corresponds to free stream static pressure, P_∞. During the two test series in the E-I Tunnel, pressures sensed by the static ports on each of the compensated pitot-static tubes, Models "C" and "D", were measured with respect to the same wall tap. Pressure differentials, $P_s - P_w$, sensed by the appropriate static ports on survey Model S-139 at $\alpha = 0°$ were then subtracted from pressure differentials with respect to the wall tap sensed by static ports on the other models to obtain pressure deviation from free stream static, $P_s - P_\infty$. Because static ports on the survey model are expected to have a small angle of attack variation of their own with the same trend and magnitude as shown on Figure 16, flow irregularities off the tunnel centerline appear small and no attempt was made to correct for residual variations in the angle of attack data for the other test models.

-16-

Schlieren photographs taken during the tests showed that the Model S-139 bow shock waves reflected from the tunnel walls intersected the model far downstream of the static ports for each Mach number with the exception of $M = 1.45$ where the reflections intersected the model in the vicinity of the S_2 and S_3 ports. Pressure variations at $M = 1.45$, Figure 16(A), show especially large deviations at the S_3 ports both at $\alpha = 0°$ and at angles of attack. To obtain an indication of free stream static pressure at $M = 1.45$ for the S_2, S_3, and S_4 port locations, a previous wind tunnel centerline survey, Reference 11, was used. Static pressure sensed by the S_1 ports, located upstream of the reflections, was considered true and deviations in centerline Mach number for the other three sets of ports were found. Corrected pressure levels for the S_2, S_3, and S_4 ports at $\alpha = 0°$ are given in Table I. These corrected values of $(P_s - P_w)/P_w$ at $M = 1.45$ were used to correlate sensed pressure for the other test models to free stream conditions.

TABLE I

Corrected Pressures at Static Ports
on Survey Model S-139
For Zero Degrees Angle of Attack
and Mach Number of 1.45

	$(P_s - P_w)/P_w$	
Static Port	First Test Series	Second Test Series
S_1	-0.0488*	-0.0508*
S_2	-0.0589	-0.0609
S_3	-0.0623	-0.0643
S_4	-0.0523	-0.0543

* Measured Data for S_1 ports was used as a base.

Data for Model S-139 from both test series are shown on Figure 16. Most test conditions, Mach number and angle of attack combination, were repeated one or more times for each test series. The connecting lines on Figure 16 show the average of all data points at each test condition. Although the second test series was run about 2-1/2 months after the first series, agreement between the two is for the most part within the estimated wind tunnel accuracy of $\Delta P/P = \pm 0.0044$, from Section 3.1.4. The average values of $(P_s - P_w)/P_w$ on Figure 16 for each test series were used to relate to free stream conditions the pressures sensed by the other test models run during the corresponding test series.

Supersonic static pressure errors for S_2 ports on the short survey tube, Model S-104, are shown on Figure 17. Absolute pressure errors for the S_1 and S_3 ports are not shown because corresponding locations, to enable determination of true static pressure, were not available on the long survey tube S-139. However, errors present at the S_2 ports are of special interest because their location is identical to that of the S_1/S_2 ports on the Type "D" models. The pitot nose on Model S-104 is also identical to that used on the Type "D" models. Pressure errors shown on Figure 17(A) would therefore be the errors present on the Type "D" models if their forward tapers and compensating afterbodies were omitted. Pressure errors at zero degrees angle of attack for the S_2 ports on Model S-104 are also presented in Table II. Converted to compressible pressure coefficient, $(P_s - P_\infty)/q_c$, these errors are indeed small as shown on Table II.

TABLE II

Supersonic Static Pressure Errors of S_2 Ports on Model S-104

M_∞	q_c/P_∞	$(P_{S_2} - P_\infty)/P_\infty$	$(P_{S_2} - P_\infty)/q_c$
1.45	2.228	+ 0.0023	+ 0.0010
2.00	4.641	- 0.0220	- 0.0047
2.50	7.526	- 0.0160	- 0.0021
3.00	11.061	- 0.0221	- 0.0020
4.00	20.064	- 0.0487	- 0.0024

-18-

Static pressure angle of attack variation of the S_2 ports on Model S-104 shown on Figure 17(B), are small and follow the same general trends that were observed for the long survey Model, Figure 16, with the exception of data points at $\alpha = + 12°$ for $M_\infty = 3.0$ and $\alpha = + 8°$ for $M_\infty = 4.0$. However, the relatively large errors at these two conditions are questionable and could be due to data errors rather than errors inherent of the model itself. Static ports on both Models, S-104 and S-139, were located ± 36° from the ventral axis of the models.

SECTION 4

CONTOURED-NOSE COMPENSATED PITOT-STATIC TUBES

4.1. DESIGN CONSIDERATIONS.

Four contoured-nose compensated pitot-static tube designs have been evaluated both analytically and through wind tunnel experiments. The configurations are designated Models C-38, C-39, C-98, and C-134. Specific dimensions and details for each model are given on Figure 9. Each design has a set of compensated subsonic static ports, S_1 ports, located on the rear portion of an ogive nose of the tube. The forward tip of the ogive is eliminated to form a pitot opening. A second set of ports, S_2 ports, located back on the cylindrical portion of the tubes, have no subsonic compensation and are designed to give reliable supersonic performance. A third set of ports, S_3 ports, located near the supersonic ports were designed for use in flight test evaluation of the units.

When the forward half of a body of revolution followed by a cylindrical section, as in the case of the Type "C" models, is placed in an airstream, the air flow is immediately decelerated at the tip of the body. Flow over the body is then uniformly accelerated with distance from the tip to a point on the ogive where the velocity will reach a maximum that is larger than free stream velocity. Aft of the point of maximum velocity the flow will uniformly decelerate to asymptotically reach free stream conditions some distance back on the cylindrical portion of the body, provided no further obstructions are present aft of the cylindrical portion. Flow velocity over most of the rear portion of the ogive nose is actually substantially greater than free stream velocity. The increase in velocity over the body in this region means that static pressures on the surface of the body is less than free stream or true static pressure. Magnitude of the decrease in pressure is dependent primarily on location on the body and free stream Mach number. Aerodynamic compensation is accomplished by placing static pressure sensing ports in this reduced pressure region on the ogive nose. Subsonically, if a contoured-nose pitot-static tube is

-20-

placed ahead of an air vehicle like the XB-70 pressure in the vicinity of the nose of the pitot-static tube, P_i, is higher than true static pressure P_∞; explained in Section 2 where the pressure increase, $P_1 - P_\infty$, or position error ahead of the XB-70 was analyzed. By proper selection of nose shape for the pitot-static tube and by placing the static ports in a specific location on the tube, position error ahead of the vehicle as a function of Mach number can be cancelled by the nose-induced negative pressure at the static ports.

Supersonically, position error ahead of the vehicle becomes zero and it is desirable for the static ports to sense true static pressure. However, for supersonic flow, induced pressures on the ogive nose continue to vary with Mach number and distribution of pressure with location on the nose changes from that observed subsonically. Therefore, a location on the ogive nose that will give good subsonic compensation, could have a large supersonic pressure error. It is for this reason that the supersonic S_2 ports were placed on the Type "C" models. A Mach switch would be utilized to switch from the subsonic ports on the nose to the supersonic ports as sonic conditions are reached. However, the possibility was investigated of finding a specific nose configuration that will give the desired level of subsonic negative pressure compensation and yet sense true static pressure from the S_1 ports supersonically. Subsonic and Supersonic Wind Tunnel tests on Model C-134, presented in Section 4 5, verify that such a configuration is feasible.

4 1.1   Theoretical Predictions.

Before wind tunnel models of the four designs were tested the designs were analyzed using well known linearized slender body theory, e g Reference 2 and 3 Theoretical calculations were conducted using an LGP-30 digital computer at REC to predict the level of subsonic aerodynamic compensation available and supersonic errors at the S_1 ports on the models. Influence of the rear body tapers and wind tunnel adapter were included in the calculations Wind tunnel tests were conducted at REC to determine the influence of eliminating the tip of the contoured-nose to form a pitot opening. Previous wind tunnel tests performed by NASA on contoured-nose compensated pitot-static tubes,

-21-

Reference 1, were also used for preliminary analysis of the designs. Curves showing the original theoretical predictions are shown super-imposed on experimental data plots presented for the four models in the following sections.

4.2. SUBSONIC AND SUPERSONIC WIND TUNNEL EVALUATION OF S_1 STATIC PORTS ON MODELS C-38, C-39, and C-98.

Subsonic and supersonic performance of the S_1 static ports on Contoured-Nose Compensated Pitot-Static Tube Models C-38, C-39, and C-98 as determined through wind tunnel tests are shown on Figures 18, 19, and 20 respectively. Models C-38 and C-39 were the first models developed and were designed to compensate for position errors ahead of the XB-70 when installed on the standard nose boom. Pressures sensed by the S_1 ports on Models C-38 and C-39 were expected to be in error supersonically and the use of a Mach switch to switch from the subsonic S_1 ports to the supersonic S_2 ports was contemplated. Model C-38 was designed for small supersonic errors at the S_1 ports under typical supersonic cruise conditions. Model C-39 was designed for small supersonic errors at the S_1 ports under transonic flow conditions enabling a smooth transition when switching from the S_1 to the S_2 ports occurs.

Subsonic performance of the S_1 ports on Model C-38 for zero degrees angle of attack is shown on Figure 18(A). Experimental data, obtained in the AEDC One Foot Transonic Model Tunnel, agrees very well with the theoretical prediction for aero-dynamic compensation. Supersonic performance, Figure 18(B) also agrees well with theory up to the maximum test Mach number of 1.5. Predicted supersonic pressure errors, extended to M = 3.0 on Figure 18(B), are shown to pass through zero at $M_\infty = 2.2$ and reach a maximum of $(P_{S_1} - P_\Delta)/P_\infty = +0.08$ at $M_\infty = 3.0$. Angle of attack perform-ance of the S_1 ports on Model C-38, Figure 18(C), shows a general increase in sensed pressure with increasing angle of attack over the Mach number range tested. The ports were located at $\pm 37\text{-}1/2°$ from the ventral centerline of the tube.

Subsonic and transonic data for the S_1 ports on Model C-39, was obtained in the Langley 8-Foot Transonio Tunnel. Experimental data at $\alpha = 0°$, Figure 19(A), was more positive than predicted values for subsonic compensation by more than one

-22-

percent at the higher subsonic Mach numbers As shown on Figure 12, this was not due to dimensional variations Transonic data to $M_\infty = 1.2$, Figure 19(B), was also more positive than the predicted values. With reference to Figure 19(C) angle of attack performance of the S_1 ports on Model C-39, located at the same $\pm 37\text{-}1/2°$ angular positions as on Model C-38, showed an increase in sensed static pressure with increasing angle of attack somewhat greater than shown for Model C-38

Although Models C-38 and C-39 were both manufactured at the same time and sent to Langley Field for testing, Model C-38 had a plugged static line and only Model C-39 was tested. Model C-38 was tested at a later date at AEDC. Because only the data for C-39 was originally available, it was assumed that the level of subsonic compensation for the Type "C" models was lower than the level predicted by theory. Using the difference between the predicted compensation and experimental compensation shown on Figure 19(A) a new unit Model C-98, was designed to give the level of compensation originally expected from the Model C-39 and needed for compensation of position error ahead of the XB-70 utilizing the standard nose boom Subsonic data for Model C-98 at $\alpha = 0°$ from tests in the AEDC Transonic Tunnel is shown on Figure 20(A) Compensation provided by the S_1 ports was larger than expected based on the discrepancy in the Model C-39 data explained above and actually agreed very well with the theoretical prediction of absolute compensation for the unit Predicted supersonic errors for the Model C-98 shown on Figure 20(B) agree reasonably well with the predicted errors However, the magnitude of the errors, necessitated by the increase in subsonic compensation needed, are large.

Because of angle of attack dependancy of the S_1 ports on Models C-38 and C-39, illustrated on Figures 18(C) and 19(C), a wind tunnel program was conducted at REC to determine what angular positioning would be needed to make static ports located on a contoured-nose insensitive to angle of attack variations. An arrangement with four static ports placed around the circumference of the tube at $\pm 26°$ locations from the vertical centerline of the tube two ports on the top and two on the bottom, was found to be insensitive to angle of attack This static port arrangement was used on the Model C-98. Angle of attack performance shown on Figure 20(C) indicates that the S_1 ports on Model

-23-

C-98 were indeed insensitive to angles of attack from $-12°$ to $+12°$ over the Mach number range tested, $M_i = 0.75$ to $M_i = 1.5$. The following section includes the wind tunnel test program run by REC to determine angle of attack dependancy of various static port locations.

4.3. CHARACTERISTICS OF THE TYPE "C" MODELS DETERMINED FROM TESTS IN THE REC TRANSONIC WIND TUNNEL.

Wind tunnel tests were conducted at REC to determine some of the characteristics of the "contoured-nose" compensated pitot-static tube. An REC Model 855E was used for the tests because of its similarity to the Model C-98. A comparison of nose shapes of Models 855E and C-98 is shown on Figure 21. The nose contours for the two models are very similar and the static ports for each model are in essentially the same location, 1.860 inches and 1.849 inches aft of the pitot opening for the 855C and C-98, respectively.

Althoug the REC tunnel is too small to obtain accurate measurements of absolute values of pressure compensation, useful results were obtained using the pressure difference method. This is a method whereby the differential is measured between the static port pressure, P_s, of the pitot-static tube and the reference pressure, P_r, at a flush wind tunnel wall tap. The absolute pressure at the wall tap is insensitive to small changes in location of the pitot-static tube in the tunnel. Data was obtained by taking the difference in $(P_s - P_r)/P_r$, or $\Delta(P_s - P_r)/P_r$, as the shape of the Model 855E or locations of the static pressure ports were modified. An indication of the residual pressure differential between the wall tap and the static port on the 855E when the tube is at a zero degree angle of attack is shown on Figure 22. Although this pressure differential behaves in a manner similar to the actual compensation provided by the Model 855E, $(P_s - P_i)/P_i$, their magnitudes are not identical. The pressure P_i is the indicated pressure at the position of the 855E static ports ahead of the aircraft on which it is used. The ratio, $(P_s - P_r)/P_r$, shown on Figure 22 is approximately 25 percent below $(P_s - P_i)/P_i$. However, this will not effect the accuracy of the data taken because the absolute values of pressure difference, $(P_s - P_r)/P_r$, are cancelled

out when the pressure differential method is used.

4 3 1 <u>Pressure Errors Induced by Varying the Diameter of the Static Pressure Ports</u>.

Relatively large static pressure ports, compared to dimensions of the contoured nose shape. are needed to assure no appreciable pressure loss through the ports under transient pressure conditions which occur when an aircraft is in a dive or climb Tests were run at REC to determine if the static port size could introduce an error in the theoretical determination of compensation induced pressure The results are shown as Figure 22 An increase in static port size from 0.020" diameter to the 0 0625" diameter used on the Type "C" models produced only minute pressure changes Increasing the port diameter induced a negative pressure error of only about $\Delta(P_s - P_r)/P_r = -0\ 0004$ with no pronounced variations with Mach number or changes in angle of attack from $-4°$ to $+4°$

4 3 2 <u>Effect of Pitot Opening on Level of Compensation Available at the Static Ports</u>

Cutting off the complete ogive nose of a "contoured-nose" pitot-static tube to make a pitot opening increased the pressure sensed at the static port. i e . reduces the compensation available at the ports This pressure increase does not lend itself to accurate prediction using theoretical methods REC conducted wind tunnel tests on the Model 855E both with and without a pitot opening The results are shown on Figure 23(A) for static ports displaced ± 33° from the ventral plane of the tube and on Figure 23(B) for port displacements of ± 45 5° from the ventral plane The positive pressure difference for zero angle of attack increases from about + 1 percent to + 7 percent of static pressure as the Mach number increases from 0 3 to 0 7 The pressure difference is also seen to vary with angle of attack and angle of displacement of the static ports from the pitot-static tube's ventral plane It becomes slightly more positive with increasing angles of attack when $\theta = \pm 33°$ and more negative with increasing angles of attack with $\theta = \pm 45\ 5°$

4 3 3 <u>Effect of Circumferential Angle Location of Static Ports on Static Pressure</u> <u>Change Induced by Angle of Attack</u>

The subsonic wind tunnel tests conducted at Langley Field indicated that subsonic S_1 ports on the Model C-39 pitot-static tube were sensitive to angle of attack. Figure 19(C) There was a pronounced change in pressure for angle of attack changes in the

small range from $-4°$ to $+4°$ and the overall change of $(P_{s_1} - P_i)/P_i$ with α was larger than desired.

In order to find an optimum circumferential location for static ports on the Model C-98, REC conducted a series of wind tunnel tests at a Mach number of 0.5. Results of the tests are shown on Figure 24. One static port, 0.0625" in diameter, was drilled in the 855E test model and data was obtained by rotating the model about its axis in the wind tunnel. Angular displacement from the ventral plane of the tube is designated as θ. A miscalculation of θ when the tests were run is the reason why the true θ angles shown on Figure 24 are given in half degree angles. There is apparent agreement between data obtained at Langley Field for $\theta = 37.5°$, Figure 19(C), and the data shown on Figure 24. Pressure difference $(P_{s_\alpha} - P_{s_{\alpha = 0°}})/P_r$, which is the ordinate parameter on Figure 24, is seen to vary over a wide range with changing θ for both positive and negative angles of attack.

A large slope through $\alpha = 0°$ is present for all θ angles. This indicates there will always be a relatively large change in pressure, P_s, for small changes in α near $\alpha = 0°$, i.e., $\alpha = \pm 4°$, if a single set of ports displaced $\pm \theta$ from the ventral plane of the pitot-static tube were used. The same basic trend as shown on Figure 24 for $M = 0.5$ will be present at higher Mach numbers; although for $M > 0.5$ the magnitude of the variation of ΔP_s for a certain θ with angle of attack will be greater. As shown on Figure 24, the optimum $\pm \theta$ location for a single set of static ports would be somewhere between $\theta = 40.5$ and 45.5, or approximately at $\theta = 41°$. This would not be a great improvement over the $\theta = 37.5°$ location that was used on Models C-38 and C-39.

A static port arrangement of two ports on the top of the tube and two ports on the bottom of the tube with each port displaced an equal angle from the vertical centerline can eliminate the angle of attack variation near $\alpha = 0°$ and also greatly reduce pressure errors at larger angles of attack. As seen from Figure 24, the $\theta = 25.5°$ line is nearly symmetrical with respect to plus or minus angles of attack. When the tube is subjected to a positive α, the two ports on the bottom of the tube will be at $+ \alpha$ but the two ports on the top of the tube will be at $- \alpha$. Therefore, an average of pressures sensed by the four ports will be approximately equal to the true static pressures at $\alpha = 0°$. Tests

were run at M = 0 3. 0 5, 0.6, and 0.7 on the 855E pitot-static tube with one static port located on the top and one on the bottom of the tube. each displaced 26° from the vertical centerline and displaced 180° from each other. The results. shown as Figure 25, verify that this arrangement is insensitive to angle of attack. The residual pressure errors are extremely small and approach the accuracy that can be obtained from wind tunnel measurements. It should be noted that, because of symmetry, the errors at $-\alpha$ will be the same as for $+\alpha$

Angle of sideslip data was obtained for the same $\theta = \pm 26°$ port arrangement listed above by rotating the tube 90° in the wind tunnel. The results, shown on Figure 26, indicate that the tube does have a relatively large residual error at large angles of pure sideslip, β, but is rather insensitive for β close to 0°. Because sideslip is only a transient condition, its errors should be secondary in consideration compared to angle of attack errors. From the data shown on Figure 24. it appears improbable to design a nose compensated pitot-static tube that will be insensitive to both angle of attack and angle of sideslip. The complement of a θ angle that is insensitive to α will be sensitive to α. and the complement is the angle felt under sideslip conditions. In fact. the four port arrangement at $\theta = \pm 26°$ appears to be the best angle of sideslip arrangement because it introduces small errors when β is near zero degrees. The pressure errors due to sideslip are also equal for either plus β or minus β. A limited amount of rerun data on Figures 25 and 26 indicates agreement of the data within .05 percent $\Delta P/P$, the accuracy stated for the tunnel in Section 3 1.5.

It should be mentioned that pure angle of sideslip for aircraft is highly improbable. Whenever there is a sideslip condition. the aircraft will also be at an angle of attack. In most cases, a small angle of sideslip will be accompanied by a relatively large angle of attack. This will form a resultant flow vector impinging the pitot-static tube at an angle near a true angle of attack. The pure sideslip case shown on Figure 26 is therefore the extreme case, with most flight maneuvers with sideslip producing pressure errors between those shown on Figures 25 and 26, but most probably close to the small angle of attack pressure error. Tests were run at a Mach number of 0 5 to determine

static pressure errors due to combined angle of attack and angle of sideslip. The data is shown as Figure 27. Errors are presented in terms of $\Delta(P_s - P_r)/P_r$ using zero angle of incidence as the reference or zero pressure differential condition. The angle of flow impingement, with respect to the vertical centerline of the tube, under combined α and β is designated as ϕ. The angle of flow incidence, with respect to the axial centerline of the tube, is equal to angle of attack when $\phi = 0°$ and equal to angle of sideslip when $\phi = 90°$. For $\phi = 0°$ (pure α), $\phi = 10°$ ($\alpha = 9\beta$), and $\phi = 20°$ ($\alpha = 4.5\beta$), the resulting pressure errors are extremely small. Beyond $\phi = 20°$, the errors appear to increase nearly linearly with increasing to $\phi = 90°$ or pure angle of sideslip. However, because combined angle of attack and angle of sideslip conditions beyond $\phi = 45°$ are highly improbable, the 26° angular position of the static ports will have small pressure errors for combined α and β under normal flight conditions. The static pressure errors for this port arrangement are the same for either positive or negative angles of incidence and are essentially zero for small angles of incidence.

It can be concluded that the ± 26° location for the four subsonic static ports on the Type "C" Models will give satisfactory results for both pure angle of attack and combined angle of attack – angle of sideslip conditions. Insensitivity for Model C-98 under pure angle of attack conditions was verified from tests at AEDC, Figure 20(C).

4 4. CIRCUMFERENTIAL ANGLE LOCATION OF STATIC PORTS ON TYPE "D" MODELS.

An extension of the wind tunnel program presented in the previous section, Section 4.3, was conducted at REC to determine angle of attack sensitivity of static ports located at various circumferential angles on a cylindrical tube and if the sensitivity was similar to that encountered for static ports located on a "contoured-nose".

The investigation was also conducted to determine if a four static pressure port arrangement would be feasible for use on a cylindrical pitot-static tube and on the Type "D" design which has its static ports located on a slight taper. A standard REC Model 852 uncompensated pitot-static tube was used in the test program. The Model 852 is an Air Force Type MA-1 and has its external dimensions specified in MIL-P-25632B. There are two sets of static ports on the MA-1. They are displaced 0.500" from each other and each port of each

set is displaced ± 37-1/2° from the ventral centerline of the tube. The forward set of ports is located 8.125" from the pitot nose of the MA-1. For test purposes three of the static ports were plugged and only one port in the forward set was used to sense static pressure. By rotating the tube in the wind tunnel mounting fixture the angle of this port from the effective tube ventral centerline, designated in this report as θ. could be varied. The procedure used in testing was identical to the procedure explained in Section 4.3. A flush wind tunnel wall tap was used to measure a reference static pressure. The differential between this pressure and the pressure sensed by the tube static port was used to find pressure variations at the static port due to changes in angle of attack, α, and static port angle, θ.

The static pressure change induced by angle of attack for circumferential θ angles from 20° to 37.5° is shown on Figure 28A and M = 0.5 The errors throughout the θ range are extremely small, but definite trends are apparent. Probable accuracy of the data. as determined from repeatability of the test data given in Section 4 3 is $\Delta P/P = \pm$ 0005. The pressure variation at $\theta = 37.5°$ is representative of performance of the Air Force Type MA-1 and TRU-1/A pitot-static tubes. To find the angle of attack influence of diametrically opposite static ports, the plus and minus angle of attack data shown on Figure 28(A) was averaged; results are shown on Figure 28(B). Because of static port symmetry. the data will be identical for plus or minus angles of attack

Angle of attack pressure variations for rotation angles of $\theta = 23°$, 26°, and 37.5° were also determined at M = 0 6 The data is presented as Figures 28(C) and 28(D). The plus angle of attack variation for $\theta = 37.5°$ is essentially the same for M = 0 5, Figure 28(A), and M = 0 6 Figure 28(C). The data for diametrically opposite static ports at M = 0 5. Figure 28(B). and M = 0 6, Figure 28(D). show that for $\theta = 23°$. 26° and 37.5° the magnitude of pressure error at angle of attack are only slightly larger for M = 0.6.

A comparison of the data at M = 0.5 and M = 0.6 indicate that a diametrically opposite static port arrangement with $\theta = 26°$ will have pressure errors at angle of attack that are comparable, actually smaller at the larger angles of attack. with the $\theta = 37.5°$ static port arrangement used on the Type MA-1 Pitot-Static Tube. The pressure errors at angle of attack are small for both cases. It is also of interest

-29-

to note that the diametrically opposite port location of $\theta = 26°$ shown on Figures 28(B) and 28(D) have the same pressure error magnitude at angle of attack as did the same port arrangement on the contoured nose of the Model 855E, Figure 25. This apparently indicates that this port arrangement is relatively insensitive to changes in the pitot-static tube contour in the vicinity of the static port. The data on Figures 28(A) and 28(D) shows that a θ angle of approximately 22° for diametrically opposite ports would actually give a smaller angle of attack variation of the pressure error in the Mach number range tested. However, from transonic wind tunnel testing at AEDC and NASA both the Type "C" and Type "D" designs with two static ports on the bottom only had a definite increase in sensed static pressure with angle of attack at $M_i = 0.95$. It is felt that by letting the sensed static pressure go slightly negative with increasing angles of attack for Mach numbers less than 0.9, the pressure increase at $M_i = 0.95$ could be eliminated. This assumption was verified by the angle of attack data obtained at AEDC for Model C-98, Figure 20(C). For Model C-98 the negative pressures, if present, were so small the wind tunnel tests at AEDC could not detect them.

To obtain an indication of angle of attack pressure variations that would be available by varying the rotation angle, tests were run at $M = 0.5$ for $\theta = 0°$, 60°, and 90°. The results are shown on Figure 28(E). The average error values for the plus angles of attack errors of Figure 28(E), i.e., the pressure errors for diametrically opposite ports, are shown on Figure 28(F).

4.5. SUBSONIC AND SUPERSONIC WIND TUNNEL EVALUATION OF S_1 STATIC PORTS ON MODEL C-134.

Model C-134 was designed to provide small supersonic errors at the subsonically-compensated S_1 ports. The four static port arrangement developed by REC, Section 4.3, and verified subsonically through wind tunnel tests on Model C-98, Section 4.2 was used on Model C-134 to check supersonic sensitivity of the S_1 port to angle of attack. The four S_1 ports were located ± 26° from the vertical centerline with two ports on the top of the tube and two ports on the bottom.

Subsonic performance of the S_1 ports at $\alpha = 0°$ is shown on Figure 29(A). The level of subsonic compensation was designed to be only slightly lower than the design

compensation of Model C-39 within $\Delta P/P_i = 0025$ in the high subsonic Mach number range. Subsonic wind tunnel data for Model C-134, obtained in the AEDC One Foot Transonic Model Tunnel, indicated a slightly lower level of compensation than that predicted from theory.

Supersonic errors for the S_1 ports at $\alpha = 0°$ are shown on Figure 29(B). Theory predicted a constantly increasing error above $M_\infty = 1.75$. However, the experimental data actually broke away from the theoretical curve and showed extremely small static pressure errors at $M_\infty = 2.5$ and 3.0. The discrepancy between theory and experiment at these higher Mach numbers is believed to be caused primarily by the blunt pitot opening for which pressure errors could not be determined accurately through theoretical analysis. Transonic data from $M_\infty = 1.0$ to 1.5 from tests in the AEDC One Foot Transonic Tunnel show reasonably good agreement with the theoretical prediction of static pressure error. Data obtained in the AEDC E-I Supersonic Wind Tunnel indicate that the supersonic errors at the S_1 ports were extremely small at all four test Mach numbers $M_\infty = 1.45$, 2.0, 2.5 and 3.0. The errors in terms of $\Delta P/q_c$ will actually be decreasing with increasing Mach number above $M_\infty = 2.0$.

Subsonic and supersonic angle of attack variations for the S_1 ports on Model C-134 are given on Figure 29(C). Subsonically, the four static port arrangement is shown to be essentially independent on angle of attack variations to $12°$. Supersonic α variations at $M_\infty = 1.20$, 1.5, 2.0, 2.5, and 3.0 are also shown to be very small. They are the same magnitude or smaller than angle of attack errors for static ports on a cylindrical pitot-static tube. e g , S_2 ports on Survey Model S-104 shown on Figure 17(B). Because of symmetry of the Model C-134 static ports, they will be as insensitive to negative angles of attack as they are to positive angles. The data on Figure 29(C) therefore applies for angles from $\alpha = -12°$ to $\alpha = +12°$.

4.6 SUBSONIC AND SUPERSONIC WIND TUNNEL EVALUATION OF S_2 AND S_3 STATIC PORTS ON THE TYPE "C" MODELS.

The S_2 static ports on the Type "C" Models are uncompensated subsonically and were designed to indicate true static pressure at supersonic Mach numbers. Models

C-39, C-98, and C-134 had the S_2 ports located on a long 0.5° tapered section in the center of the tube, Figure 9. The S_2 ports on Model C-38 were located on an untapered cylindrical section. There were two basic reasons for placing the S_2 ports on a 0.5° body taper. The taper increases the strength of the tube and also will induce a small positive pressure supersonically to cancel the slight negative pressure effect induced by the pitot nose. A third set of ports, S_3 ports, was placed one inch ahead of the S_2 ports on Model C-98 and were designed for use as a flight test reference. Pressures measured by the S_3 ports would be essentially identical to those sensed at the super-sonic S_2 ports.

Experimental data for the S_2 and S_3 ports are shown on Figure 30. Subsonic errors with respect to indicated static pressure, Figure 30(A), are well within one percent with the exception of data obtained in the Langley 8-Foot Transonic Tunnel which went over one percent at $M_i = 0.9$, 0.95, and 1.0. Agreement between data run in the AEDC tunnel was very good for all three models which indicates eliminating the 0.5° body taper on Model C-38 had little influence on sensed static pressure. Pressures measured by the S_2 and S_3 ports on Model C-98 are also shown to be identical. Supersonic data on Figure 30(B) for the S_2 ports on Model C-134 indicate only small errors at the four test Mach numbers, from $M_\infty = 1.45$ to 3 0. Subsonic and supersonic angle of attack performance of the S_2 and S_3 ports, Figure 30(C), show little or no variation of sensed pressure with angle of attack over the α range tested.

4.7. SUMMARY OF AERODYNAMIC PERFORMANCE OF THE TYPE "C" PITOT-STATIC TUBES.

(1) Based on a comparison of wind tunnel data for the four Type "C" models evaluated under this program and theoretical predictions of negative pressure com-pensation provided by the S_1 ports on the models, it can be concluded that the level of aerodynamic compensation can be predicted with reasonable accuracy using theoretical methods. Of the three models tested at AEDC, experimental results agree within $0 \leq \Delta P/q \leq 0.01$ or within one percent of the calculated values over a Mach number range from $0.55 \leq M \leq 0.90$. The compensating nose design on

-32-

Model C-38 was found to give the desired level of subsonic compensation necessary for use with the standard nose boom on the XB-70.

(2) Through an extensive study it was found that for static ports located on the contoured nose a four port arrangement, two ports located on the top of the tube and two on the bottom with each port displaced equally from the vertical centerline, is more satisfactory for obtaining insensitivity to angle of attack variations than is a two static port arrangement with each port displaced equal angles from the ventral plane of the tube. This was found to be true for the $\pm 26°$ four port arrangement used on Model C-134 over an angle of attack test range, from $-12°$ to $+12°$, for both subsonic and supersonic flight to $M_\infty = 2.5$ and to $\alpha = \pm 8°$ at $M_\infty = 3.0$. Static pressure errors due to angle of attack over this range remained primarily well within 0.5 percent of q

(3) A nose design was found for Model C-134 that would give a desirable level of subsonic compensation at the S_1 ports and yet the S_1 ports could be continued in use through the supersonic Mach number range to 3.0 with less than a 0.5 percent of q error in static pressure from $M_\infty = 2.0$ to $M_\infty = 3.0$

(4) The supersonic S_2 ports and reference S_3 ports on all four models measured very nearly the indicated static pressure subsonically and sensed true static pressure supersonically. The S_2 and S_3 ports, located $\pm 36°$ from the ventral plane of the pitot-static tube were insensitive to angle of attack changes both subsonically and supersonically.

(5) Pitot pressure measurements were also made during all the wind tunnel tests. The pitot opening design was identical for all four models and indicated at all angle of attack conditions run, the true total pressure subsonically and true pitot pressure. total pressure behind a normal shock wave supersonically. Any deviations of data from the true pitot pressure were of a random nature and therefore due to measurement limitations of the wind tunnel facilities. Although pitot pressure errors do exist at high angles of attack the errors over the α range used in the preset test series. $-4° \le \alpha \le +13.43°$ for the Langley 8-Foot Transonic Tunnel and $0° \le \alpha \le +12°$ for the AEDC tunnels. were too small to be recorded on the measuring equipment used Pitot errors to $\alpha = \pm 14°$ are expected to be well within $\Delta P_p / P_p = \pm 0.001$ both subsonically and supersonically

-33-

(6) Of the configurations investigated, the Model C-134 would match the expected static pressure aerodynamic compensation for the XB-70 aircraft at a location 71 inches forward of the nose. Accuracy of the compensated static pressure would be within $\pm$ .01 q for the subsonic range $0.5 \lessgtr M_i \lessgtr 0.95$ and the supersonic range $1.5 \lessgtr M_i \lessgtr 3.0$ for angles of attack within $\pm 12°$ (except $\pm 8°$ at $M_\infty = 3.0$). Accuracies in the $1.0 \lessgtr M_i \lessgtr 1.5$ range were not accurately established, but available data indicate errors in this range should not exceed $\pm$ .03 q.

CONTOURED AFTERBODY COMPENSATED PITOT-STATIC TUBES

5.1. DESIGN CONSIDERATIONS AND THEORETICAL PREDICTIONS.

Seven aerodynamically compensated pitot-static tubes utilizing the "contoured-afterbody" method* of static pressure compensation have been evaluated using both theoretical analysis and wind tunnel experiments. They were designated the Type "D" models and specific dimensions for each model are given on Figure 10. A single set of static ports, S_1/S_2, was used to compensate for subsonic position error ahead of the aircraft and to indicate true static pressure supersonically. The S_1/S_2 ports are located on a slight taper which extends forward to the 7-1/2° pitot nose taper and rearward to a maximum diameter of 0.744 inches at 0.062 inches behind the static ports. The compensating afterbody contour starts 0.062 inches behind the static ports and has an inflecting curvature which starts and ends tangent to the flow direction. The length of the compensating contours and the slope along the contour was varied to provide various levels of subsonic compensation. The afterbody contour accelerates the flow and produces a reduced static pressure region. Subsonically this pressure influence is propagated forward to the static ports. Supersonically after the aircraft's bow shock wave has passed downstream of the static ports, the pressure influence of the afterbody contour is isolated from the static ports, thus providing no supersonic compensation. In addition to the afterbody contour, the pitot opening, forward taper, and rear adapter tapers also provide subsonic pressure influences at the S_1/S_2 ports. All of these parameters were evaluated theoretically for each of the models developed. An example of predicted pressure influences of each component on Models D-41, D-123, D-147, and D-159 is shown on Figure 31. These four models had identical external configurations with the exception of placement of the static ports. The afterbody contour, Curve (D), provides the largest portion of subsonic compensation. However,

* REC Patent Pending

the 0.72° forward taper, Curve (C), also induces a large negative pressure at the static ports. Because of remoteness of the S_1/S_2 ports from the pitot nose, the pitot opening and nose taper effect, Curve (B), is of negligible importance. The rear adapter tapers produce positive pressures. Curve (A) on Figure 31 is an accumulation of the pressure effects of the 6° rear taper which increases the tube diameter from 0.620" to 1.312" and the 7-1/2° taper on the wind tunnel adapter. A summation of pressure influences from all the individual components, Curve (E), is the total compensation provided by the S_1/S_2 ports. Pressure effects of the pitot opening and rear tapers are hard to predict accurately because of limitations of theory. However, the total effect of these components is small and even a 25 percent error in theoretical prediction would not cause an appreciable error in the level of compensation provided. To minimize the uncertainty of pressure from the rear tapers, imperical relationships were also used to obtain a more accurate indication of variation with Mach number. The forward taper and afterbody contour are the basic components for providing aerodynamic compensation because of their immediate proximity to the static ports. The pressure influence of both of these components are easily determined through slender-body theory.

At supersonic Mach numbers the pitot nose and forward taper influence the pressure at the S_1/S_2 ports. The total nose effect is small but negative. Each of the Type "D" designs has a forward taper to produce a slight positive pressure and thereby cancel the pitot nose effect.

A second set of static ports, S_3 ports, were placed one inch ahead of the S_1/S_2 ports on five of the Type "D" models. The S_3 ports were designed to sense indicated static pressure subsonically and true static pressure supersonically. As on the Type "C" models, the S3 ports will be used as a reference for flight test evaluation of the aircraft static pressure systems.

5.2. SUBSONIC AND TRANSONIC WIND TUNNEL EVALUATION OF COMPENSATED STATIC PORTS ON MODEL D-40.

Models D-40 and D-41 were the first two afterbody compensated pitot-static tubes developed under this contract. They were designed for use on the standard nose boom of the XB-70. The S_1/S_2 static ports on Model D-40 were located two inches further

from the pitot opening than on the other six Type "D" models tested and a 0 52° forward taper was used to increase the tube diameter from 0.610 inches to 0 7.44 inches Two S_1/S_2 ports were used with each port displaced ± 36° from the bottom centerline of the model.

Wind tunnel data for Model D-40 was obtained in the Langley 8-Foot Transonic Tunnel. Subsonic and transonic performance of the S_1/S_2 ports at $\alpha = 0°$ is shown on Figure 32(A) Although the predicted compensation agreed well with experimental data at $M_i = 0.4$, at high subsonic Mach numbers the experimental data was lower than expected from the theoretical analysis. Transonic data at $M = 1\ 05$, 1.1, and 1.2 indicated a negative residual static pressure error

Angles of attack performance of the S_1/S_2 ports on Model D-40, Figure 32(B), indicates insensitivity of the static ports to $M_i = 0.90$. From $M_i = 0.95$ to $M_\infty = 1.20$, the sensed static pressure increases with increasing angle of attack

5.3. SUBSONIC WIND TUNNEL EVALUATION OF STATIC PORTS ON MODEL D-102.

Subsonic wind tunnel data for Model D-41 at $\alpha = 0°$, from tests obtained at the same time as Model D-40 in the Langley 8-Foot tunnel. also indicated a lower level of static pressure compensation than expected from theoretical analysis. To obtain the level of subsonic compensation needed for use with the standard nose boom, a new design, Model D-102, was developed for testing in the AEDC One Foot Transonic Tunnel. The desired level of compensation was estimated by subtracting the difference in predicted and experimental levels of subsonic compensation for Model D-41 from the absolute level of predicted compensation for the Model D-102. However, a comparison between predicted and eventual experimental values on Figure 23(A) shows that the wind tunnel data at $\alpha = 0°$ was actually larger than the absolute level predicted from theory at low Mach numbers. The difference decreased with increasing Mach number to $M_i = 0.95$ where the wind tunnel data equals the predicted level of compensation. As shown on Figure 23(A), the difference remained within 1/2 percent of $(P_{s_1/s_2} - P_i)/P_i$, stated accuracy of the AEDC Transonic Tunnel. throughout the subsonic Mach number range. The Model D-102 therefore will have more subsonic compensation then needed when used with the standard nose boom on the XB-70.

-37-

Angle of attack performance of the S_1/S_2 ports, located $\pm 36°$ from the ventral centerline on Model D-102, is shown on Figure 33(B). Some sensitivity to angle of attack was observed at $M_i = 0.95$.

Subsonic performance of the reference static ports on Model D-102 is shown on Figure 33(C) for $\alpha = 0°$ and on Figure 33(D) for angle of attack variations. The S_3 ports had a negative error with respect to indicate static pressure which reached a maximum of $(P_{S_2} - P_i)/P_i = -0.016$ at $M_i = 0.95$ for $\alpha = 0°$. Angle of attack variation for the S_3 ports, located at the same angular location as the S_1/S_2 ports, did not show the increase in pressure with angle of attack at $M_i \cong 0.95$ that was observed for the S_1/S_2 ports.

5.4. SUBSONIC AND SUPERSONIC WIND TUNNEL EVALUATION OF STATIC PORTS ON MODELS D-41, D-123, D-147, AND D-159.

Models D-41, D-123, D-147, and D-159 had identical compensating contours and the same external dimensions with the exception of their static port arrangements. As shown on Figure 10, the S_1/S_2 ports on Models D-41 and D-123 were placed $\pm 36°$ from the bottom centerline. Model D-123 also incorporated a set of S_3 ports with the same circumferential $\pm 36°$ location. Models D-147 and D-159 had four S_1/S_2 ports and four S_3 ports arranged around the circumference of the tubes at $\pm 26°$ and $\pm 24°$ from the vertical centerline, respectively. The static ports were placed on a $0.72°$ forward taper for all four models. Model D-159 was evaluated only at supersonic Mach numbers.

5.4.1. Evaluation of S_1/S_2 Ports at Zero Degrees Angle of Attack.

Because of dimensional similarity subsonic and supersonic performance of the S_1/S_2 ports or S_3 ports for the four models should be identical at zero degrees angle of attack. Subsonic and transonic static pressure compensation provided by the S_1/S_2 ports on Models D-41, D-123, and D-147 is shown on Figure 34(A). Four sets of wind tunnel data from two wind tunnel facilities are shown. Model D-41 was first tested in the NASA Langley 8-Foot Transonic Tunnel and later tested in the AEDC tunnel. Data from both of these tests showed a lower level of subsonic compensation

than that predicted theoretically. Data obtained for Model D-41 at AEDC was about 0.5 percent of $(P_{s_1/s_2} - P_i)/P_i$ closer to the theoretical prediction than the NASA data at the higher subsonic Mach numbers. Additional tests at AEDC on Models D-123 and D-147 gave even higher levels of subsonic compensation and for the case of D-123, the data was larger than the predicted level of compensation throughout the entire subsonic range.

The reason for the discrepancy between the four sets of subsonic data on Figure 34(A) has not been determined. Stated accuracies for the Langley 8-Foot tunnel were $\Delta P/P_i = \pm 0.0016$ at $M_i = 0.4$ increasing to $\Delta P/P = \pm 0.0027$ at $M_i = 1.0$, Section 3.1.1. and stated accuracies for the AEDC one foot tunnel were $\Delta P/P_i = 0.005$ throughout the subsonic range, Section 3.1.3. Dimensional variations for the three models were shown on Figure 13 to be generally considerably less than $\Delta P/P_i = \pm 0.002$. Assuming these accuracies the maximum deviation of the data at $M_i = 0.95$ could be only $\Delta P/P_i = 0.012$.

After the Model D-41 had been tested at NASA and AEDC, a decision was made to use the extended nose boom on the XB-70 and that a Type "D" compensated pitot-static tube would be used. The static pressure error at the S_1/S_2 ports located 71.291 inches ahead of the aircraft on the extended nose boom, as determined in Section 2, is shown superimposed on Figure 34(A). Although slightly lower than the NASA data at high subsonic Mach numbers, the predicted position error ahead of the aircraft agrees well with the NASA data especially below $M_i = 0.6$. Because the Langley 8-Foot tunnel had a larger test section and probably was more free of disturbances and flow irregularities than the AEDC tunnel and because the Langley tunnel had tighter stated data accuracies, the decision was made to use the external configuration of Model D-41, and Models D-123, D-147, and D-159, and the static port spacings of Model D-123.

It should be noted that residual error after compensation is obtained by subtracting the static pressure error ahead of the aircraft, $(P_\infty - P_i)/P_i$, shown on Figure 34(A) from the compensation provided by the S_1/S_2 ports, $(P_{s_1/s_2} - P_i)/P_i$, or $(P_{s_1/s_2} - P_\infty)$ $/P_i$. This error can then be divided by $\left[(P_\infty - P_i)/P_i\right] + 1$ to obtain $(P_{s_1/s_2} - P_\infty)/P_\infty$.

Transonic data obtained in the NASA tunnel for $M_i = 1.05$, 1.1, and 1.2 shown on Figure 34(A) indicates that compensation provided by the model drop abruptly toward zero after the bow shock wave has passed downstream of the static ports. There will, therefore, be no large deviations in sensed static pressure as the aircraft passes through the transonic region.

Three of the four models, D-123, D-147, and D-159, were evaluated super-sonically at $\alpha = 0°$. Data, shown on Figure 34(B), was taken in the AEDC E-I Supersonic Tunnel for Mach numbers from $M_\infty = 1.45$ to $M_\infty = 4.0$. Total data scatter for the models exceeds only slightly the stated accuracy for the E-I tunnel, $\Delta P/P_\infty = \pm 0.0044$ from Section 3.1.4. The data points on Figure 34(B) have been corrected for pressures sensed by the long survey model, S-139, shown on Figure 16. The connecting lines on Figure 34(B) indicate the averages of the supersonic data agree very well with the supersonic performance of the S_2 ports on the short survey model, S-104, shown on Figure 17(B). Corresponding errors in terms of $(P_s - P_\infty)/q_c$ for the survey Model S-104 and therefore for the Models presented on Figure 34(B) were very small, as was shown on Table II and discussed in Section 3.3.2

5.4.2. <u>Angle of Attack Performance of S_1/S_2 Ports on Models D-41 and D-123</u>.

Subsonic and supersonic angle of attack variations of pressure sensed by the S_1/S_2 ports on Models D-41 and D-123 are shown on Figure 34(C). The S_1/S_2 ports show very small angle of attack changes to $+13.43°$ for Mach numbers to $M_i = 0.8$. The largest deviations shown on Figure 34(C) are in the transonic region at $M_i = 0.9$, 0.95, 1.1, and 1.2. However, in this region differences in data from the two wind tunnel facilities are also the largest and a certain amount of the variation could be inherent wind tunnel errors. Importance of any residual variations in this region are actually minimized by the fact that large angles of attack will not normally be experienced when the aircraft passes through the transonic region. Supersonic variations with angle of attack were primarily well within $\Delta P/P_\infty = 0.02$ for Mach numbers to 3.0. Because of the favorable angle of attack performance of the S_1/S_2 ports on Models D-41 and D-123, their port arrangement was used on the compensated pitot-static tubes furnished for use on the XB-70.

-40-

5.4.3. <u>Evaluation of S_3 Ports at Zero Degrees Angle of Attack.</u>

Subsonic and supersonic static pressure errors of the S_3 reference ports on Models D-123, D-147, and D-159 are shown on Figures 34(D) and 34(E). The S_3 ports are located one inch ahead of the S_1/S_2 ports and were designed to sense indicated static pressure, P_i, subsonically and true static pressure, P_α super- sonically. Subsonic variations from indicated pressure are within $(P_{S_3} - P_i)/P_i =$ -0.01 as indicated on Figure 34(D) for Models D-123 and D-147. Agreement between the two models is good. Supersonic errors with respect to true static pressure, Figure 34(E), are small for all three models, D-123, D-147, and D-159. Agreement of supersonic data between the three models is also very good.

5.4.4. <u>Angle of Attack Performance of S_3 Ports on Model D-123.</u>

Subsonic and supersonic angle of attack variation for the S_3 ports on Model D-123 are shown on Figure 34(F). As was the case for the S_1/S_2 ports on Model D-123, the S_3 ports exhibited no large variations with angle of attack either subsonically or super- sonically. This static port arrangement, $\pm 36°$ from the ventral plane of the model, was therefore used for the S_3 ports on the compensated pitot-static tubes furnished for use on the XB-70.

5.4.5. <u>Angle of Attack Performance of S_1/S_2 Ports and S_3 Ports on Model D-147.</u>

The S_1/S_2 and S_3 ports on Model D-147 were placed around the circumference of the tube at $\pm 26°$ from the vertical centerline, two ports on the top and two ports on the bottom. This port arrangement was found to be very insensitive to angle of attack variations both subsonically and supersonically for the S_1 ports on Model C-134, Section 4.5. The wind tunnel analysis conducted by REC, Section 4.4, indicated that subsonically the "four holes at $\pm 26°$" arrangement was also insensitive to α variations for a cylindrical pitot-static tube. The static port arrangement is as insensitive to negative angles of attack as positive angles of attack thereby practically doubling the useful angle of attack range of previous static ports which were located on the bottom of the tube and were sensitive to negative angles of attack.

The model D-147 was therefore tested to verify the subsonic performance of the

-41-

"four holes at ± 26°" arrangement. Subsonic and supersonic data obtained in the AEDC wind tunnel is shown on Figure 35(A) for the S_1/S_2 ports and on Figure 35(B) for the S_3 ports. The REC subsonic test results were verified by the tests at AEDC. The static ports were found to be insensitive to angle of attack variations to $M_i = 0.95$ for angles of attack from $-12°$ to $+12°$.

Supersonically the static ports were found to be insensitive to variations from $\alpha = -4°$ to $\alpha = +4°$ and only moderate angle of attack changes were observed at $M_\infty = 1.5$ for $-12° \leq \alpha \leq +12°$. However, beyond $\alpha = 4°$ at $M_\infty = 2.0, 2.5$, and 3.0 the sensed static pressure at the S_1/S_2 and S_3 ports decreased rapidly with increasing angle of attack.

5.5. SUPERSONIC PERFORMANCE OF STATIC PORTS ON MODELS D-158 AND D-159.

Models D-158 and D-159 were designed for two basic purposes: (1) to eliminate at $\sigma = 0°$ the small supersonic static pressure errors of the S_1/S_2 and S_3 ports on Models D-123 and D-147 and (2) to find a four static port arrangement that would be insensitive to large angles of attack supersonically. The Model D-159 had the same external dimension as used on the unit supplied for use on the XB-70, i.e. the same as Models D-41, D-123, and D-147. As explained in Section 5.5.4, the "four ports at + 26°" arrangement used on Model D-147 was insensitive to subsonic angle of attack changes. Because additional subsonic tests were not available, only a modest change in static port location could be made. Location of the four S_1/S_2 and S_3 ports on Model D-159 were therefore placed at ± 24°. This change would not effect the subsonic performance significantly but, it was hoped, would reduce the supersonic variations.

Model D-158 was designed to provide better supersonic performance at $\tau = 0°$. The forward taper was increased to $1-1/4°$ and the $7-1/2°$ pitot taper was reduced in length. The static ports on Model D-158 were also located at ± 24", i.e. the same as on Model D-159. A comparison of supersonic errors of Models D-158 and D-159 at $\alpha = 0°$ is shown on Figure 36(A) for the S_1/S_2 ports and on Figure 37(A) for the S_3 ports. Increasing the forward taper from $0.72°$ on Model D-159 to $1.25°$ on Model D-158 did decrease the supersonic errors present at both the S_1/S_2 and S_3 ports except at $M_\infty = 1.45$ for the S_3 ports. In fact, assuming the characteristic shape of supersonic

-42-

errors vs. Mach number curve on Figures 36(A) and 37(A) is correct, the Model D-158 appears to be the optimum configuration for reducing supersonic errors throughout the Mach number range from M = 1.45 to M = 4.0.

Large angle of attack variations for the S_1/S_2 and S_3 ports on Models D-158 and D-159, Figures 36(B), 36(C), 37(B), and 37(C), were still present at $\alpha = \pm 8°$ and $\pm 12°$ for both models. In fact, only minor changes appear compared to the errors that were present for the S_1/S_2 and S_3 ports on Model D-147, Figures 35(A) and 35(B). It therefore appears that a significant change in hole spacing, to $\pm 20°$ or less, would have to be made to reduce these errors. However, any further reduction in angle would necessitate additional subsonic as well as supersonic verification.

5.6. SUMMARY OF AERODYNAMIC PERFORMANCE OF THE TYPE "D" PITOT-STATIC TUBES.

(1) Seven Type "D" aerodynamically compensated pitot-static tubes utilizing the "contoured-afterbody" method of static pressure compensation were evaluated using both theoretical analysis and wind tunnel experiments. Although a fair amount of wind tunnel data uncertainty exists for subsonic compensation available from the models, the level of aerodynamic compensation was predicted with reasonable accuracy using theoretical methods. Experimental results for the four models tested subsonically at AEDC agree with calculated values within one percent of q_c over a Mach number range from $0.55 \leqq M_i \leqq 0.95$.

(2) Two deiced and anti-iced pitot-static tubes have been furnished to ASD for installation on the XB-70 aircraft. They utilized the Model D-123 design and were designated the REC Model 855D aerodynamically compensated pitot-static tube. The compensated S_1/S_2 ports exhibited, based on NASA wind tunnel data, the level of subsonic compensated needed to correct the position error ahead of the aircraft when mounted on the extended nose boom. Supersonic errors for the S_1/S_2 ports were found to be small for Mach numbers to 3.0. The S_1/S_2 ports were insensitive to angle of attack variations throughout the Mach number and angle of attack capabilities of the aircraft. The S_3 reference ports on Model 855D sensed very nearly the indicated

static pressure subsonically and true static pressure supersonically and were not sensitive to angle of attack variations.

(3) An alternate static port arrangement for the S_1/S_2 and S_3 ports, four ports located ± 26° from the vertical centerline with two ports on the top of the tube and two ports on the bottom, was found to be insensitive to angle of attack variations from -12° to +12° for Mach numbers to 1.5. At Mach numbers of 2.0, 2.5, and 3.0 this port arrangement remained insensitive for angles of attack from -4° to +4°. Beyond $\alpha = \pm 4°$ the static ports showed a negative $\Delta P/q$ sensitivity with increasing angle of attack. For this reason they were not used on the final Model 855D design.

(4) Pitot pressure measurements were made during all the wind tunnel tests on the Type "D" models. The pitot opening design was identical for all seven Type "D" models and indicated the true total pressure subsonically and true pitot pressure, total pressure behind a normal shock wave, supersonically for all angle of attack conditions run. Any deviations of the true pitot pressure were of a random nature and therefore due to measurement limitations of the wind tunnel facilities. Pitot errors to ± 14° are expected to be well within $\Delta P_p/P_p = \pm 0.001$ both subsonically and supersonically.

(5) Based on the contoured-afterbody configurations evaluated under this contract, it is concluded that aerodynamic compensation can be achieved for static pressure errors at distances beyond 3 feet from the nose of the XB-70 aircraft. Accuracy of the compensated static pressure would be within ± 0.01 q_c for subsonic Mach numbers to $M_i = 0.95$ and in the supersonic range $1.5 \leqslant M_\infty \leqslant 3.0$ for angles of attack to 12° (to 8° at $M_\infty = 3.0$). Accuracies in the $1.0 \leqslant M_i \leqslant 1.5$ range were not definitely established, but available data indicates errors in this range should be well within ± 0.02 q_c.

REFERENCES

1. Ritchie, Virgil S., Several Methods for Aerodynamic Reduction of Static-Pressure Sensing Error for Aircraft at Subsonic, Near-Sonic, and Low Supersonic Speeds, NASA Report 18, 1959.

2. Spreiter, John R., and Alksne, Alberta Y., Slender-Body Theory Based on Approximate Solution of the Transonic Flow Equation, NASA Report R-2, 1959.

3. Liepmann, H.W., and Roshke, A.; Elements of Gasdynamics, John Wiley and Sons, Inc., 1957.

4. O'Bryan, Thomas C., Danforth, Edward D. B., and Johnston, J. Ford, Error in Airspeed Measurement Due to the Static-Pressure Field Ahead of an Airplane at Transonic Speeds, NACA Report 1239, 1955.

5. Wright, Ray H., Ritchie, Virgil S., and Pearson, Albin O., Characteristics of the Langley 8-Foot Transonic Tunnel with Slotted Test Section, NACA Report 1389, 1958.

6. Characteristics of Nine Research Wind Tunnels of the Langley Aeronautical Laboratory, NACA, Washington 1957.

7. Chew, William L., Jr.; PWT, ARO, Inc.,; Determination of Optimum Operating Parameters for the 1-Foot Transonic Tunnel Utilizing Cone-Cylinder Bodies of Revolution, AEDC-TN-60-69, April 1960.

8. Test Facilities Handbook, (4th Edition), Arnold Engineering Development Center, Arnold Air Force Station, Tennessee, July 1962.

9. Rittenhouse, Lewis E., Propulsion Wind Tunnel Facility ARO, Inc., Transonic Wind Tunnel Results for Five Pressure Probes Designed to Minimize Static-Pressure Sensing Errors, AEDC-TDR-62-48, March 1962.

10. White, W.E., and Martin, T.A., Transonic Investigation of Three Pitot-Static Probes Designed for Pressure-Error Compensation, AEDC-TDR-62-123, June 1962.

11. Anderson A., *Summary Report on Calibration of Tunnel E-I, A 12-inch Mach 5 Supersonic Wind Tunnel*, AEDC-TN-58-8, March 1958.

12. *Rosemount Engineering Company Transonic Wind Tunnel Facility*, REC Bulletin 106021, 21 October 1960.

13. Gracey, William, *Measurements of Static Pressure on Aircraft*, NACA Report 1364, 1958.

APPENDIX "A"

LIST OF SYMBOLS

C_p	$\Delta P / q$
M	Mach number
M_∞	True Mach number
M_i	Indicated Mach number corresponding to P_i at distance x ahead of fuselage.
ΔM	Mach number differential
$P_s = P$	Static Pressure
P_∞	True Static Pressure
P_i	Indicated or uncompensated static pressure at distance x ahead of fuselage.
$P_T = P_p$	Pitot Pressure
P_o	Total Pressure
$P_r = P_w$	Static pressure sensed by flush wind tunnel wall tap.
P_{s_1}	Pressure sensed by S_1 static ports
P_{s_2}	Pressure sensed by S_2 static ports
P_{s_1/s_2}	Pressure sensed by S_1/S_2 static ports
P_{s_3}	Pressure sensed by S_3 static ports
ΔP	Static pressure differential
q	$\dfrac{\gamma}{2} PM^2$
q_c	$P_T - P_s$
q_{c_∞}	$P_T - P_\infty$

q_{c_i}	$P_T - P_i$
S_1	Subsonic compensated static pressure ports (Except on Survey Model)
S_2	Supersonic static pressure ports (Except on Survey Model)
S_1/S_2	Subsonic and Supersonic compensated static pressure ports.
S_3	Reference static pressure ports (Except on Survey Models)
S_4	Fourth static pressure port on survey model S-139.
x	Distance ahead of aircraft
Δx	Axial increment on fuselage
α	Angle of attack, Degrees
β	Angle of sideslip, Degrees
θ	Angle of placement of static ports from vertical centerline, Degrees
ϕ	Angle of flow impingement from ventral centerline of pitot-static tube, Degrees
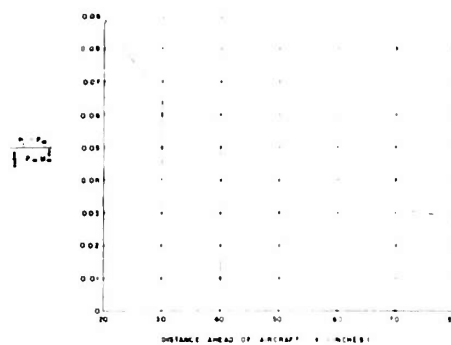
FIGURE 1
STATIC PRESSURE ERROR AHEAD OF XB-70
AT $M_\infty = 0.4$
COMPUTED USING EXACT FUSELAGE NOSE SHAPE
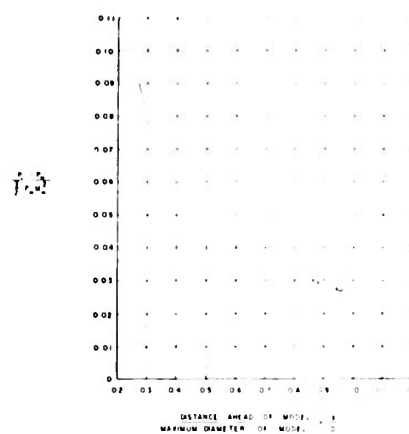
FIGURE 2A
PRESSURE DISTRIBUTION AHEAD OF SLENDER NOSE
TRANSONIC AIRCRAFT MODEL OF REFERENCE ($M_\infty = 0.4$)
COMPUTED USING EXACT NOSE SHAPE
WIND TUNNEL DATA, REFERENCE
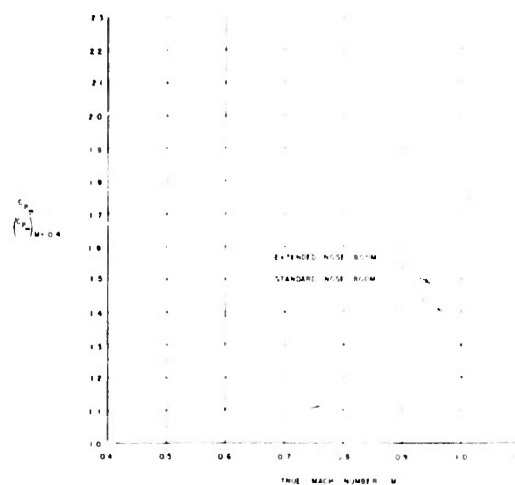
FIGURE 2B
EMPIRICAL RELATIONSHIP FOR EFFECT OF
COMPRESSIBILITY ON STATIC PRESSURE ERROR AHEAD OF XB-70

$$C_p = \frac{p - p_\infty}{\frac{1}{2} \rho_\infty v_\infty^2}$$
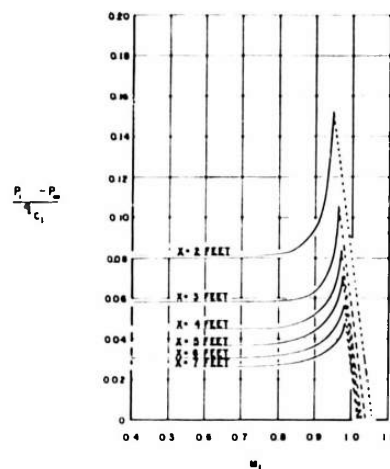
FIGURE 3

STATIC PRESSURE ERROR AHEAD OF
XB-70 AS A FUNCTION OF INDICATED
MACH NUMBER
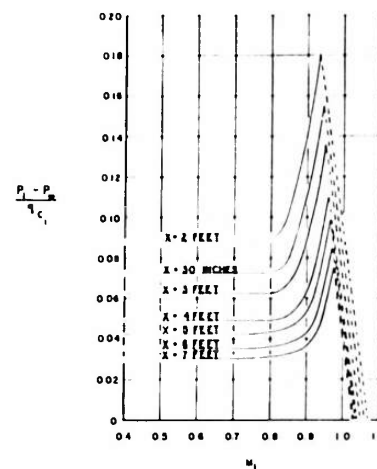
(REC ESTIMATE)

FIGURE 4

STATIC PRESSURE ERROR AHEAD OF
XB-70 AS A FUNCTION OF INDICATED
MACH NUMBER

(NAA ESTIMATE)
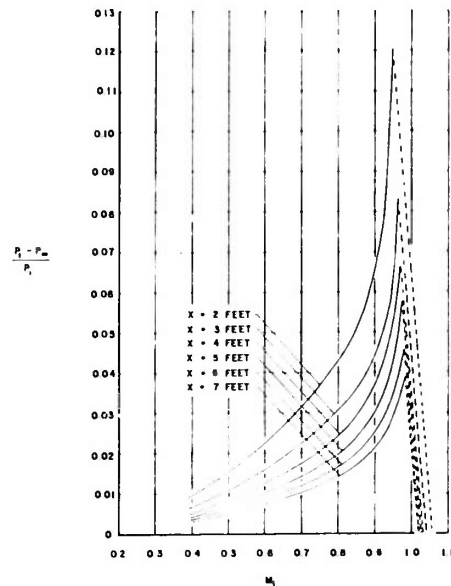
FIGURE 5

STATIC PRESSURE ERROR AHEAD OF
XB-70 AS A FUNCTION OF INDICATED
MACH NUMBER
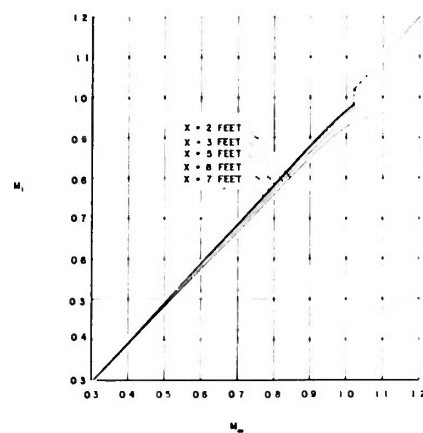
(REC ESTIMATE)

FIGURE 6

INDICATED MACH NUMBER AS A FUNCTION
OF TRUE MACH NUMBER FOR REC ESTIMATE
OF POSITION ERROR AHEAD OF XB-70
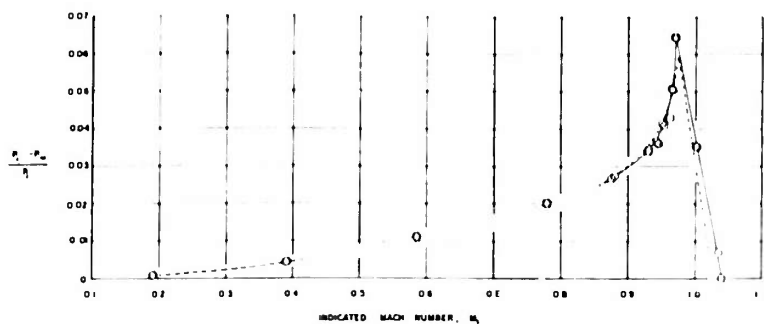
FIGURE 7(A)

STATIC PRESSURE ERROR AHEAD OF XB-70
AS A FUNCTION OF INDICATED MACH NUMBER

X = 60.951 INCHES

--- REC PREDICTION
O RESULTS OF NASA WIND TUNNEL
TESTS OR XB-70
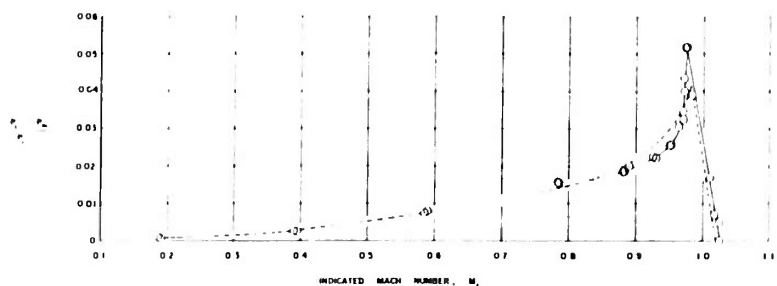
FIGURE 7(D)

STATIC PRESSURE ERROR AHEAD OF XB-70
AS A FUNCTION OF INDICATED MACH NUMBER.

X = 80.302 INCHES

--- REC PREDICTION
O RESULTS OF NASA WIND TUNNEL
TESTS OR XB-70
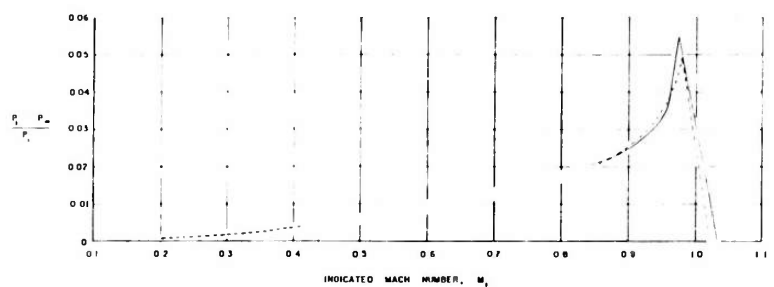
FIGURE 7(C)

STATIC PRESSURE ERROR AHEAD OF XB-70
AS A FUNCTION OF INDICATED MACH NUMBER.

X = 71.291 INCHES

--- REC PREDICTION
—— AVERAGE OF NASA WIND TUNNEL
DATA FOR XB-70 MODEL FROM
FIGURES 7A (X = 60.951") AND
FIGURE 7B (X = 80.302")

-51-
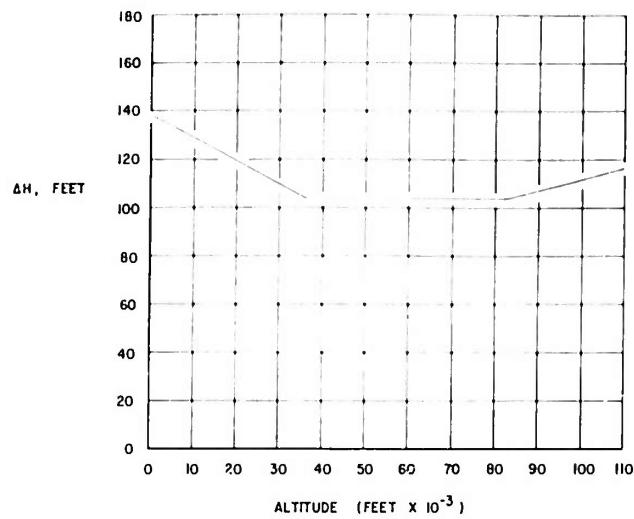
FIGURE 8 (A)

PRESSURE - ALTITUDE ERROR CORRESPONDING
TO STATIC PRESSURE ERROR OF $\Delta P/P = 0.005$.
(STANDARD ATMOSPHERIC CONDITIONS)
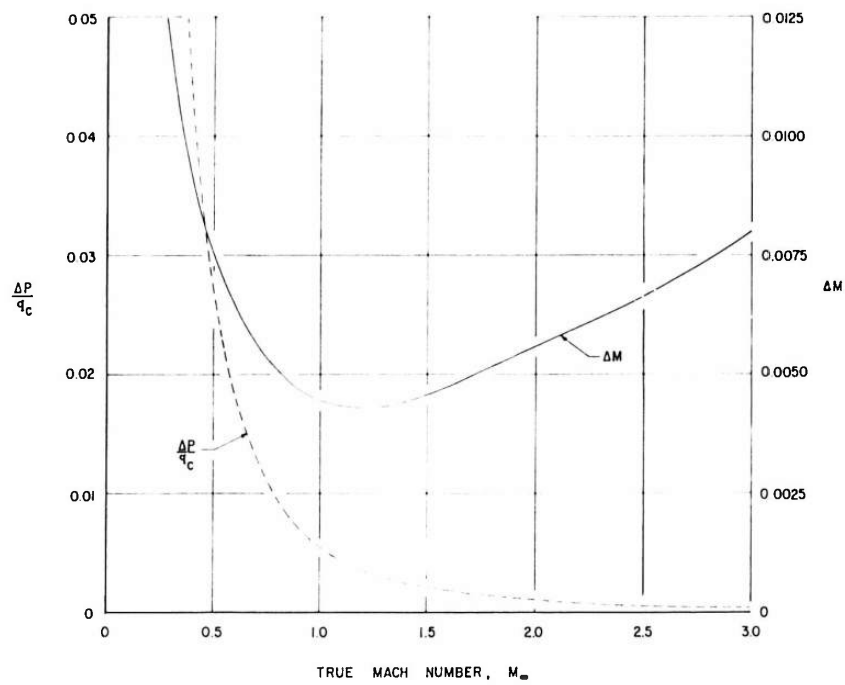
FIGURE 8 (B)

COMPRESSIBLE PRESSURE COEFFICIENT ERRORS AND
MACH NUMBER ERRORS CORRESPONDING TO STATIC
PRESSURE ERROR OF $\Delta P/P = 0.005$.
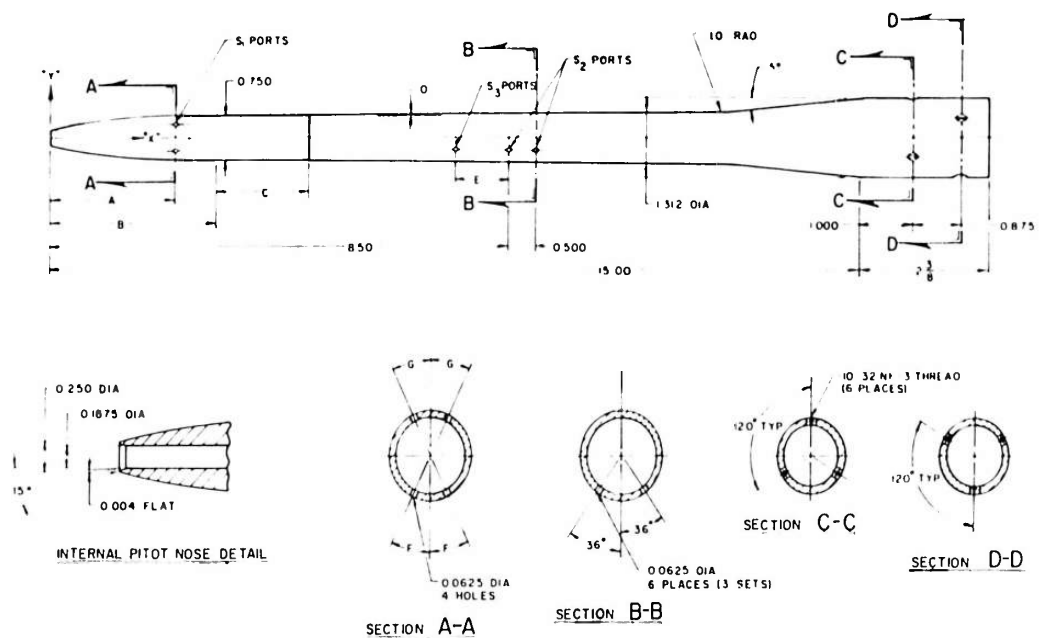
INTERNAL PITOT NOSE DETAIL

SECTION A-A

SECTION B-B

SECTION C-C

SECTION D-D

SPECIFIC MODEL DIMENSIONS

MODEL	A	B	C	O	E	F	G	COMMENTS
C-38	2312	3062					375°	
C-39	1676	2756	2000	0.5°			375°	
C-98	1849	2449	2307	0.5°	1000	26°	26°	
C-134	2086	3062	1694	0.5°		26°	26°	NO S₃ PORTS

NOSE COORDINATES

MODEL C-38 AND MODEL C-134		MODEL C-39		MODEL C-98	
x	y	x	y	x	y
0	0125	0	0125	0	0125
0 250	0164	0 250	0168	0 250	0173
0 500	0200	0 500	0207	0 500	0217
0 750	0232	0 750	0243	0 750	0255
1 000	0262	1 000	0274	1 000	0287
1 250	0287	1 250	0300	1 250	0315
1 500	0 310	1 500	0323	1 500	0337
1 750	0329	1 750	0342	1 750	0 355
2 000	0345	2 000	0356	2 000	0367
2 250	0357	2 250	0367	2 250	0373
2 500	0367	2 500	0373	2 449	0375
2 750	0372	2 756	0375		
3 062	0375				

NOTE ALL DIMENSIONS IN INCHES

FIGURE 9

DIMENSIONS AND DETAILS OF CONTOURED-NOSE
WIND TUNNEL MODELS

SPECIFIC MODEL DIMENSIONS

MODEL	A	B	C	D	E	F	G	H	COMMENTS
D-40	0.610	8.50	7.312	—	1.085	6.610	36°	—	NO S₁ PORTS, NO STATIC PORTS ON TOP OF TUBE
D-41	0.610	6.50	5.312	—	.364	6.810	36°	—	PORTS ON TOP OF TUBE
D-123	0.610	6.50	5.312	.000	.364	6.810	36°	—	NO S₁, OR S₂ PORTS NO STATIC
D-102	0.610	6.50	5.312	1.000	0.96	6.810	36°	—	PORTS ON TOP OF TUBE
D-147	0.610	6.50	5.312	.000	1.364	6.810	26°	26°	NO STATIC PORTS ON TOP OF TUBE
D-156	0.493	6.50	5.757	.000	1.364	6.810	24°	24°	
D-159	0.610	6.50	5.312	1.000	1.364	6.810	24°	24°	

NOTE: ALL DIMENSIONS IN INCHES

AFTERBODY CONTOUR COORDINATES

MODELS D-41, D-123, D-147, D-102, D-156, & D-159		MODEL D-40		MODEL D-102	
X	Y	X	Y	X	Y
0.062	0.372	0.620	0.372	0.042	0.372
0.200	0.370	0.200	0.370	0.200	0.359
0.400	0.351	0.400	0.358	0.400	0.322
0.600	0.331	0.600	0.344	0.600	0.345
0.800	0.327	0.800	0.324	0.800	0.333
1.200	0.324	1.000	0.313	0.800	0.218
1.200	0.314	1.147	0.310	.033	0.310
1.426	0.310				

SECTION A-A

SECTION B-B

SECTION C-C

INTERNAL PITOT NOSE DETAIL

FIGURE 10

DIMENSIONS AND DETAILS OF CONTOUR-AFTERBODY WIND TUNNEL MODELS

* PATENT PENDING

-54-

FIGURE 11
DIMENSIONS AND DETAILS OF WIND TUNNEL SURVEY MODELS AND WIND
TUNNEL ADAPTER
(ALL DIMENSIONS IN INCHES)
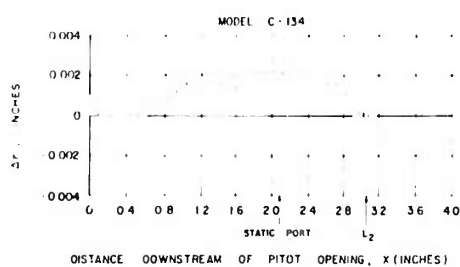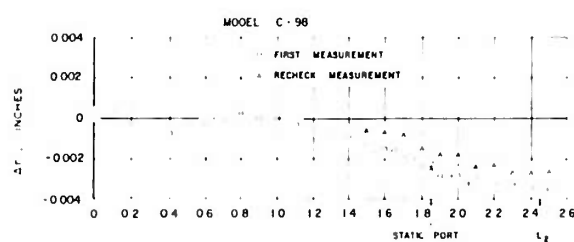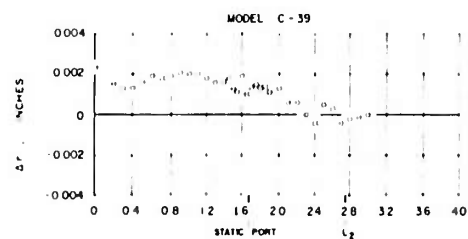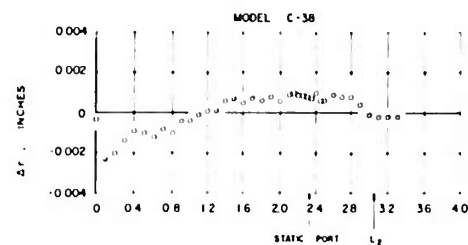
FIGURE 12(A)

DEVIATIONS OF ACTUAL RADIUS FROM
DESIGN RADIUS FOR COMPENSATING CONTOURS
FOR TYPE C MODELS

X = 0 IS START OF COMPENSATING CONTOURS
X = L₂ IS END OF COMPENSATING CONTOURS
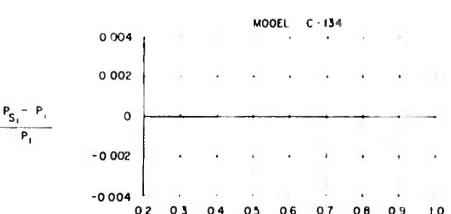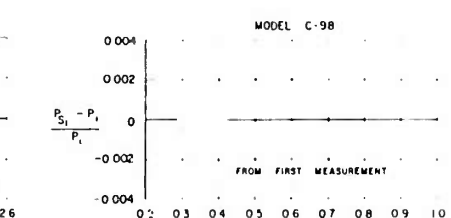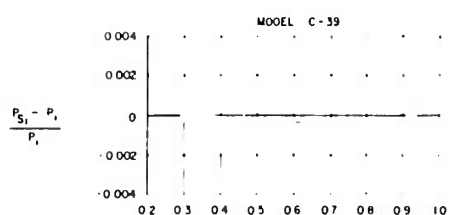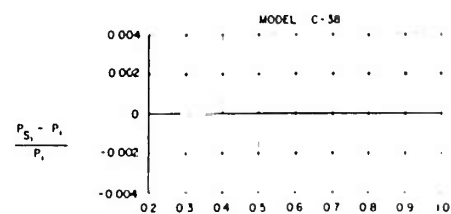
FIGURE 12(B)

APPROXIMATE STATIC PRESSURE ERROR
INDUCED BY DIMENSIONAL VARIATIONS
FROM THE DESIGN CONTOURS OF
TYPE C MODELS

P_{S_i} = PRESSURE SENSED AT COMPENSATED
STATIC PORTS

P_i = INDICATED PRESSURE AT STATIC PORTS

-56-
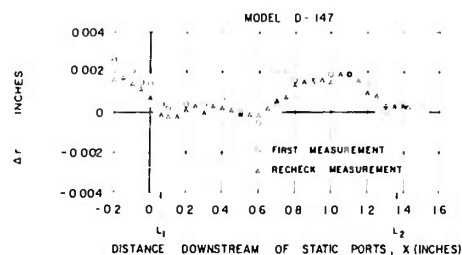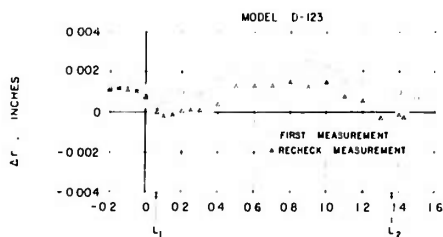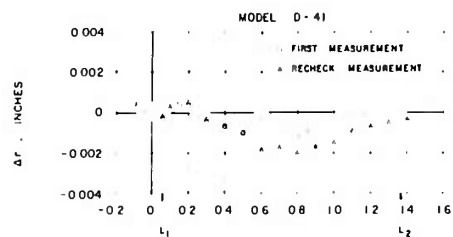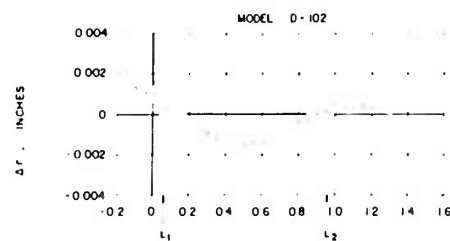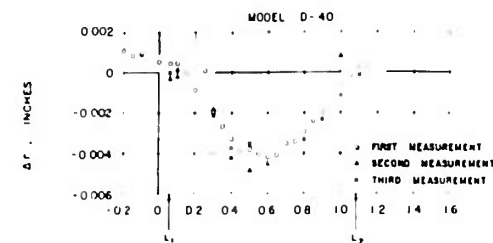
FIGURE 13(A)

DEVIATIONS OF ACTUAL RADIUS FROM
DESIGN RADIUS FOR COMPENSATING CONTOURS
OF TYPE D MODELS.

X = O IS LOCATION OF STATIC PORTS
X = L₁ IS START OF COMPENSATING CONTOURS
X = L₂ IS END OF COMPENSATING CONTOURS
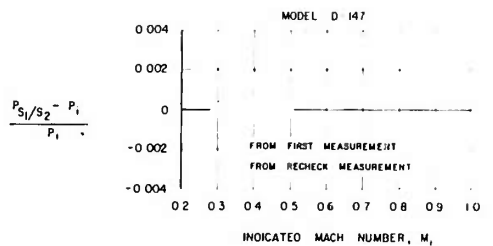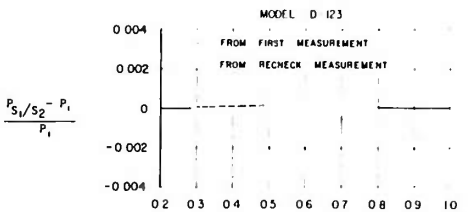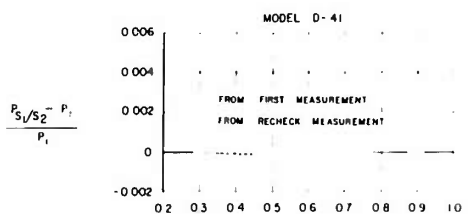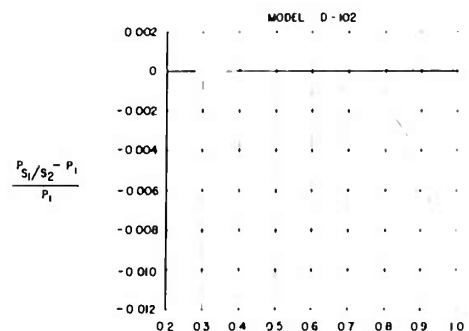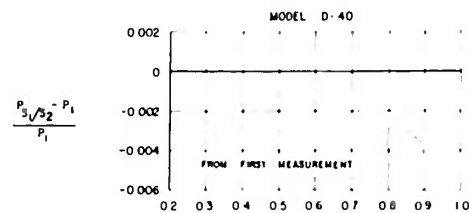
FIGURE 13(B)

APPROXIMATE STATIC PRESSURE ERROR
INDUCED BY DIMENSIONAL VARIATIONS
FROM THE DESIGN CONTOUR OF
TYPE D MODELS.

P_{S_1/S_2} = PRESSURE SENSED AT
COMPENSATED PORTS
P_1 = INDICATED PRESSURE AT
STATIC PORTS

-57-
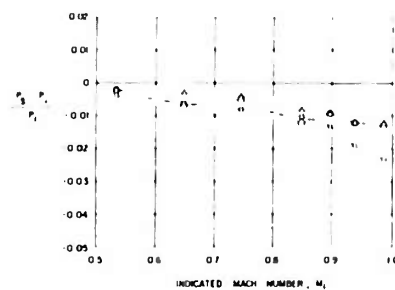
FIGURE 14 (A)

SUBSONIC PERFORMANCE OF STATIC PORTS

ON SURVEY MODEL S-104.

$\alpha = 0°$

(EXPERIMENTAL DATA AEDC ONE FOOT TRANSONIC

MODEL TUNNEL)

S_1 STATIC PORTS

$\wedge$ S_2 STATIC PORES

" S_3 STATIC PORTS

FIGURE 14 (B)

ANGLE OF ATTACK PERFORMANCE

OF STATIC PORTS ON SURVEY

MODEL S-104

(EXPERIMENTAL DATA AEDC ONE FOOT

TRANSONIC MODEL TUNNEL)

S_1 STATIC PORTS

$\wedge$ S_2 STATIC PORTS
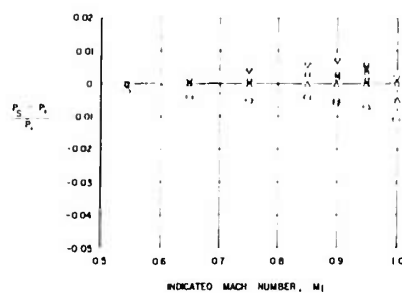
" S_3 STATIC PORTS

FIGURE 15 (A)

SUBSONIC PERFORMANCE OF STATIC PORTS

ON SURVEY MODEL S-139.

$\alpha = 0°$

(EXPERIMENTAL DATA - AEDC ONE FOOT TRANSONIC

MODEL TUNNEL)

S_1 STATIC PORTS

$\wedge$ S_2 STATIC PORTS

" S_3 STATIC PORTS
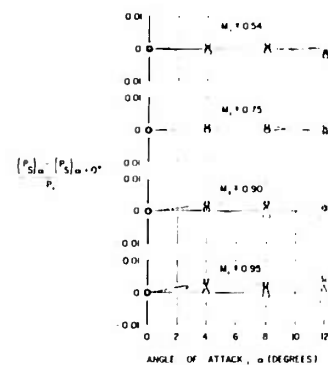
$\vee$ S_4 STATIC PORTS

FIGURE 15 (B)

ANGLE OF ATTACK PERFORMANCE

OF STATIC PORTS ON SURVEY

MODEL S-139

(EXPERIMENTAL DATA AEDC ONE FOOT

TRANSONIC MODEL TUNNEL)
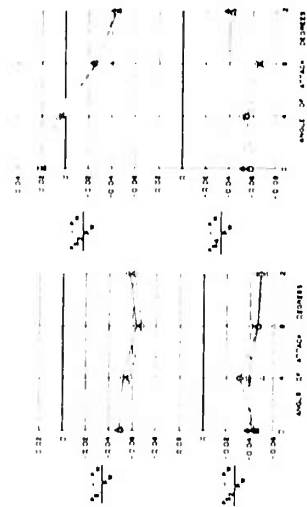
S_1 STATIC PORTS

$\wedge$ S_2 STATIC PORTS

S_3 STATIC PORTS

S_4 STATIC PORTS
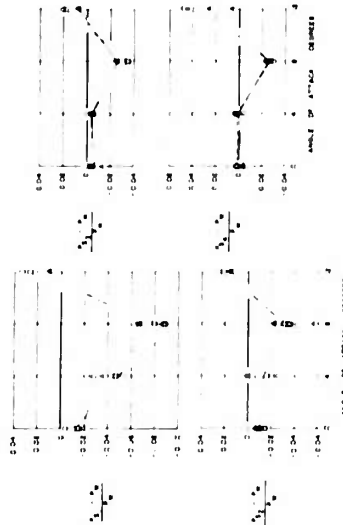
FIGURE 6

PRESSURE SENSED BY STATIC PORTS ON SURVEY MODEL 3-39

DATA OBTAINED IN AEDC E-1 SUPERSONIC WIND TUNNEL.

△ FIRST TEST SERIES
□ SECOND TEST SERIES
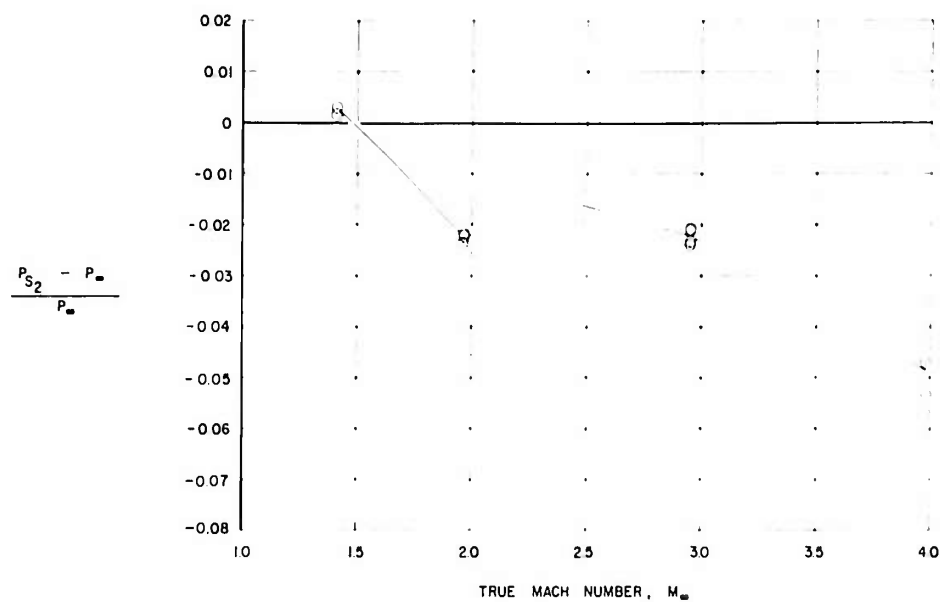
FIGURE 17 (A)

SUPERSONIC PERFORMANCE OF S_2 STATIC PORTS ON SURVEY
MODEL S - 104.

$\alpha = 0°$

EXPERIMENTAL DATA: (AEDC E-I SUPERSONIC WIND TUNNEL)
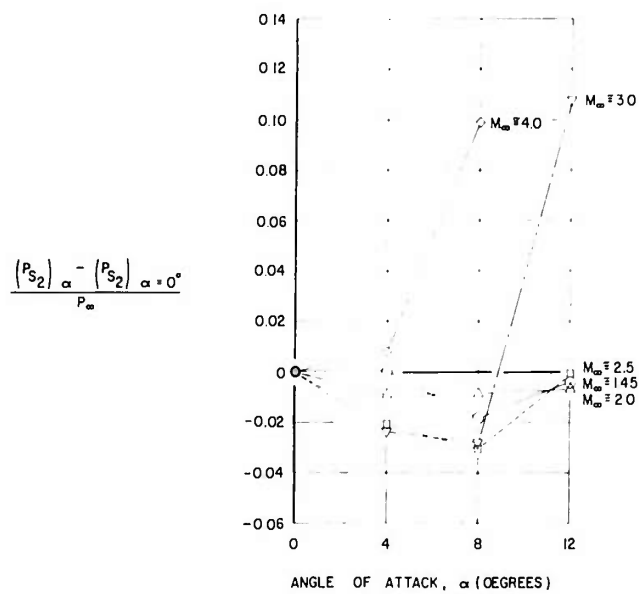
FIGURE 17 (B)

ANGLE OF ATTACK PERFORMANCE

OF S_2 STATIC PORTS ON SURVEY

MODEL S-104.

EXPERIMENTAL DATA :

(AEDC E-I SUPERSONIC WIND TUNNEL)

-60-

FIGURE 19(a)
SUBSONIC PERFORMANCE OF 5 STATIC PORTS ON MODEL C 38
α = 0°
EXPERIMENTAL DATA
(AEDC ONE FOOT TRANSONIC MODEL TUNNEL)
THEORETICAL PREDICTION
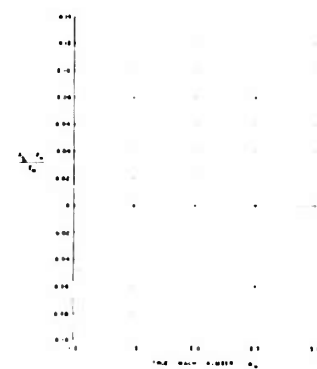
FIGURE 19 b
SUPERSONIC PERFORMANCE OF 5 STATIC PORTS
ON MODEL C 38
α = 0°
EXPERIMENTAL DATA
(AEDC ONE FOOT TRANSONIC MODEL TUNNEL)
THEORETICAL PREDICTION

FIGURE 19 c
ANGLE OF ATTACK PERFORMANCE OF 5 STATIC PORTS ON MODEL C 38
EXPERIMENTAL DATA (AEDC ONE FOOT TRANSONIC MODEL TUNNEL)

FIGURE 19(a)
SUBSONIC PERFORMANCE OF 5 STATIC PORTS ON MODEL C 38
α = 0°
EXPERIMENTAL DATA
(LANGLEY 8 FOOT TRANSONIC TUNNEL)
THEORETICAL PREDICTION
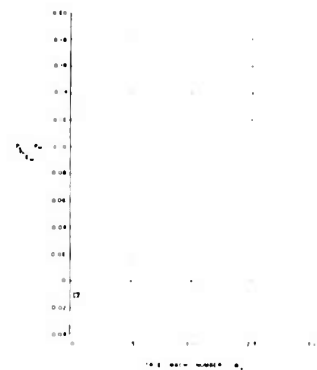
FIGURE 19 b
SUPERSONIC PERFORMANCE OF 5 STATIC PORTS ON
MODEL C 38
α = 0°
EXPERIMENTAL DATA
(LANGLEY 8 FOOT TRANSONIC TUNNEL)
THEORETICAL PREDICTION

FIGURE 19 c
ANGLE OF ATTACK PERFORMANCE OF 5 STATIC PORTS ON MODEL C 38
EXPERIMENTAL DATA (LANGLEY 8 FOOT TRANSONIC TUNNEL)
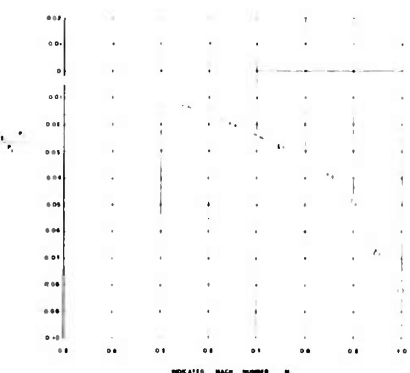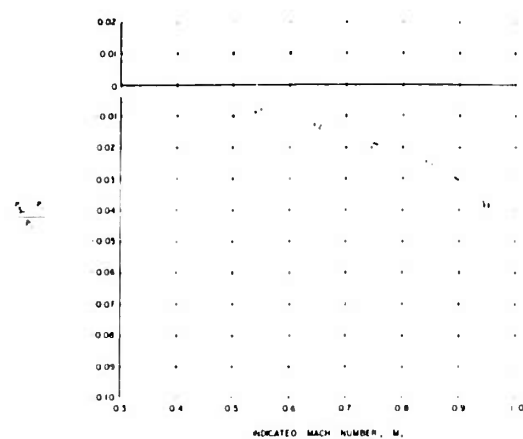
FIGURE 20(a)
SUBSONIC PERFORMANCE OF 5, STATIC PORTS ON MODEL C 38
α = 0°
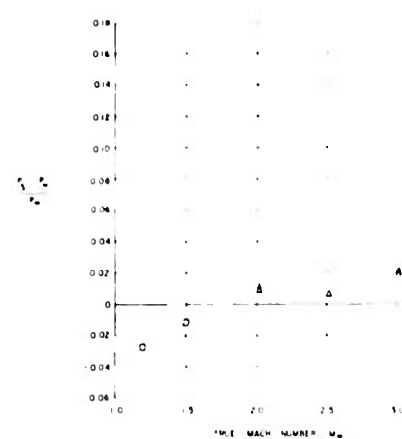EXPERIMENTAL DATA
(AEDC ONE FOOT TRANSONIC MODEL TUNNEL)
THEORETICAL PREDICTION
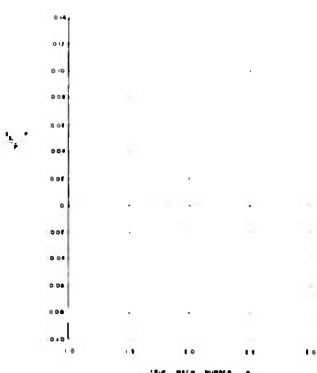
FIGURE 20 b
SUPERSONIC PERFORMANCE OF 5 STATIC PORTS
ON MODEL C 38
α = 0°
EXPERIMENTAL DATA
(AEDC ONE FOOT TRANSONIC MODEL TUNNEL)
THEORETICAL PREDICTION
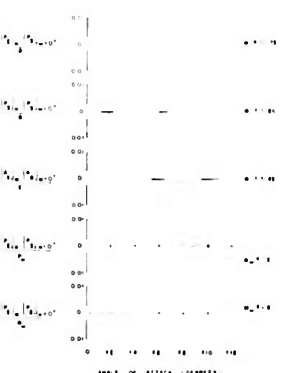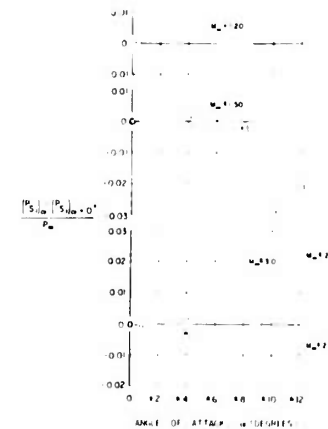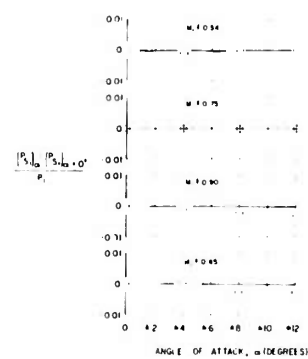
FIGURE 20 c
ANGLE OF ATTACK PERFORMANCE OF 5, STATIC PORTS ON MODEL C 38
EXPERIMENTAL DATA (AEDC ONE FOOT TRANSONIC MODEL TUNNEL)
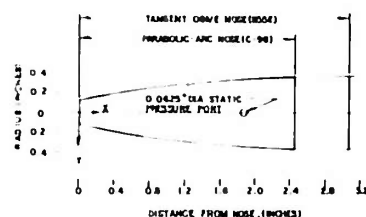
FIGURE 21

COMPARISON OF NOSE SHAPES OF NEC MODEL C-98
AND B55E COMPENSATED PITOT STATIC TUBES.

STATIC PORTS ARE LOCATED AT X=1.860" FON THE
B55E AND AT X=1.849" FOR THE C-98.
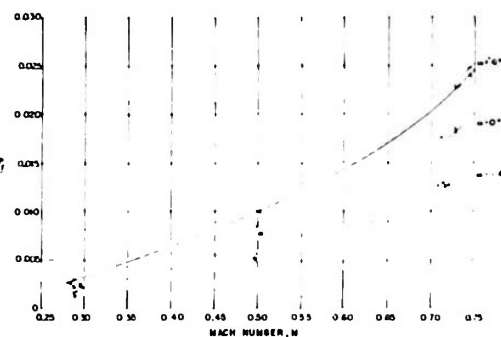
FIGURE 22

STATIC PRESSURE CHANGE INDUCED BY CHANGING THE SIZE OF THE SUBSONIC
STATIC PORTS ON A MODEL B55E.

STATIC PORTS ARE LOCATED ±35° FROM THE VENTRAL PLANE OF
THE TUBE.

     STATIC PORT DIAMETER = 0.0625"
     STATIC PORT DIAMETER = 0.020".
P_s = PRESSURE SENSED AT STATIC PORTS.
P_r = REFERENCE PRESSURE FROM FLUSH WINO TUNNEL WALL TAP.
α = ANGLE OF ATTACK.
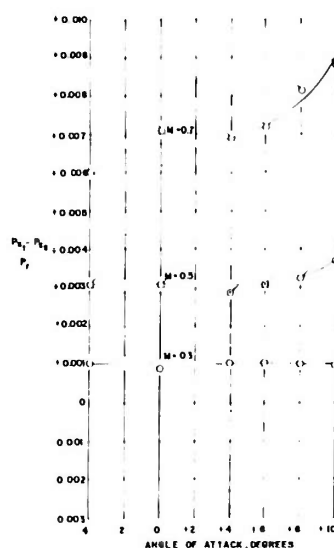
FIGURE 23(A)

STATIC PORTS LOCATED ±33° FROM THE VENTRAL
PLANE OF THE TUBE
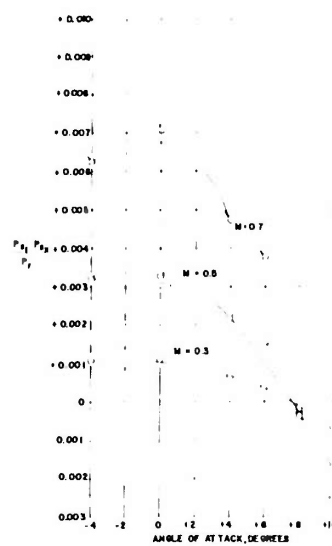
FIGURE 23(B)

STATIC PORTS LOCATED ±45.5° FROM THE
VENTRAL PLANE OF THE TUBE

FIGURE 23

PRESSURE INCREASE AT STATIC PORTS OF A MODEL B55E WHEN THE FORWARO
PORTION OF THE FULL TANGENT OGIVE NOSE IS CUT OFF TO MAKE A PITOT
OPENING.

P_{s_1} = PRESSURE SENSEO AT STATIC PORTS OF BODY WITH PITOT OPENING.
P_{s_2} = PRESSURE SENSEO AT STATIC PORTS OF BODY WITH COMPLETE TANGENT OGIVE NOSE
P_r = REFERENCE PRESSURE FROM FLUSH WINO TUNNEL WALL TAP.
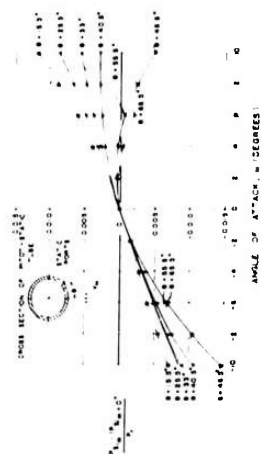
FIGURE 24

EFFECT OF CIRCUMFERENCE ANGLE LOCATION
OF REC MODEL B55 E STATIC PORTS ON
STATIC PRESSURE CHANGE INDUCED BY ANGLE
OF ATTACK (M=0.5)

p_s : PRESSURE SENSED BY STATIC PORT
p_r : REFERENCE PRESSURE FROM FLUSH WALL TAP
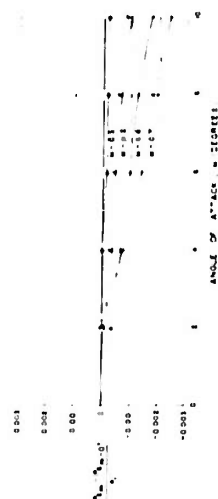
FIGURE 25

STATIC PRESSURE ERROR DUE TO ANGLE
OF ATTACK FOR REC MODEL B55 E STATIC
PORTS LOCATED ON THE TOP AND
ON THE BOTTOM OF THE TUBE. EACH
PORT DISPLACED ±26° FROM THE VERTICAL
CENTERLINE

☆ RERUN DATA CHECK AT M=0.8
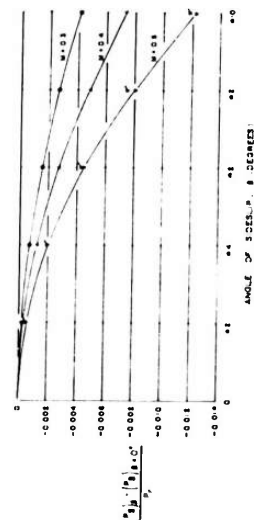
FIGURE 26

STATIC PRESSURE ERROR DUE TO ANGLE OF
SIDESLIP FOR REC MODEL B55 E. STATIC PORTS
LOCATED ON THE TOP AND ON THE
BOTTOM OF THE TUBE. EACH PORT DISPLACED
±26° FROM THE VERTICAL CENTERLINE

☆ RERUN DATA CHECK AT M=0.8
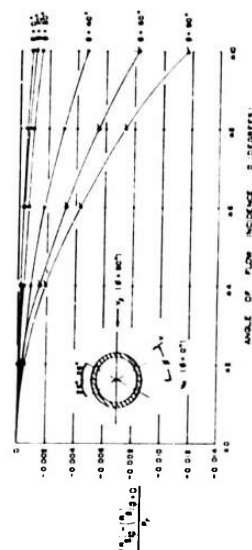
FIGURE 27

STATIC PRESSURE ERROR DUE TO COMBINED
ANGLE OF ATTACK AND ANGLE OF SIDESLIP
FOR REC MODEL B55 E STATIC PORTS
LOCATED ON THE TOP AND ON THE BOTTOM
OF THE TUBE, EACH PORT DISPLACED ±26°
FROM THE VERTICAL CENTERLINE (M=0.5)

FOR β=0°, THE ANGLE OF FLOW INCIDENCE WILL BE
ANGLE OF ATTACK, α
FOR α=90°, THE ANGLE OF FLOW INCIDENCE WILL BE
ANGLE OF SIDESLIP, β

-63-
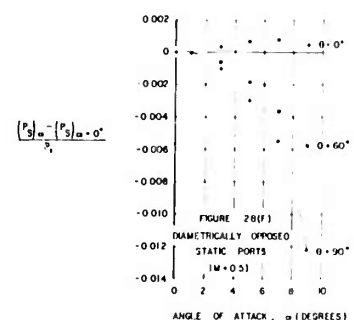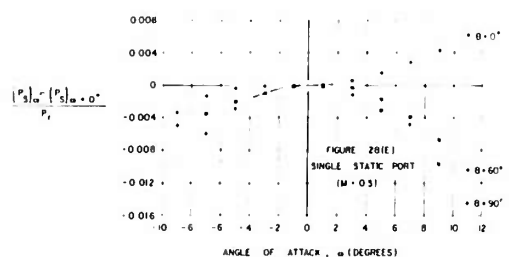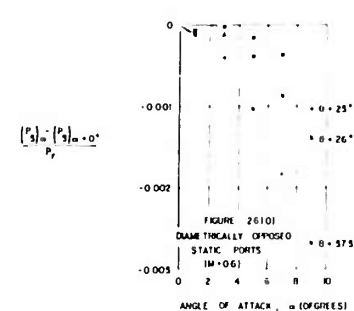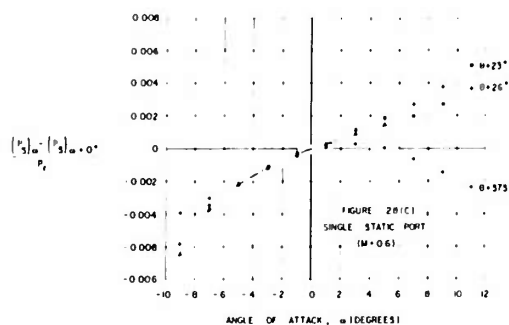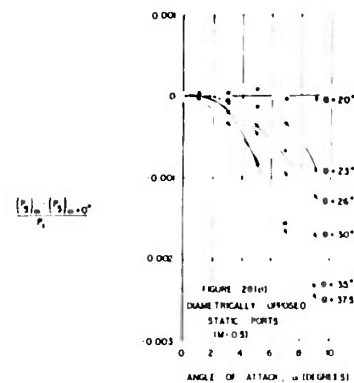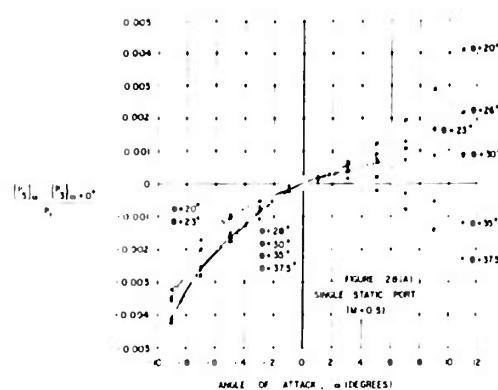
FIGURE 28

EFFECTS OF CIRCUMFERENTIAL ANGLE LOCATION OF STATIC PORTS ON STATIC
PRESSURE CHANGE INDUCED BY ANGLE OF ATTACK.
(MA-I PITOT STATIC TUBE)
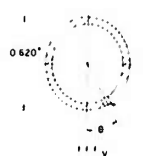
FIGURE 29(A)

SUBSONIC PERFORMANCE OF S_i PORTS ON MODEL C-134

$\alpha = 0°$

EXPERIMENTAL DATA

(AEDC ONE FOOT TRANSONIC MODEL TUNNEL)

THEORETICAL PREDICTION

FIGURE 29(B)
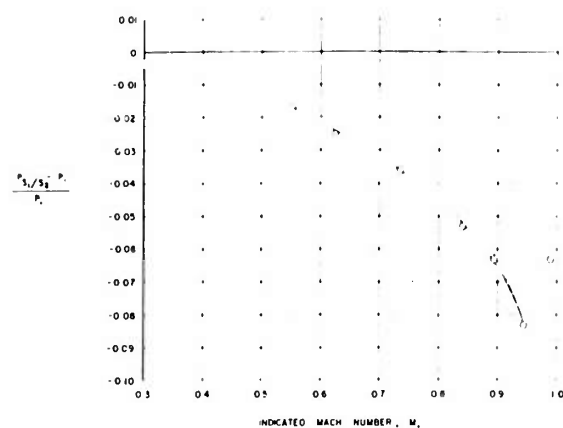
SUPERSONIC PERFORMANCE OF S STATIC

PORTS ON MODEL C-134

$\alpha = 0°$

EXPERIMENTAL DATA

(AEDC ONE FOOT TRANSONIC MODEL TUNNEL)

△ (AEDC E I SUPERSONIC WIND TUNNEL)

THEORETICAL PREDICTION

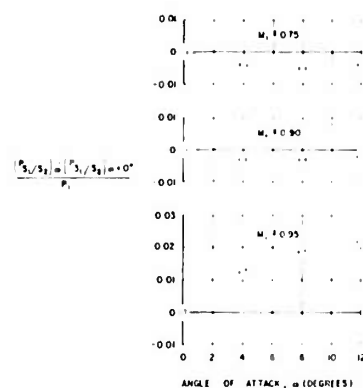FIGURE 29(C)

ANGLE OF ATTACK PERFORMANCE OF S_i STATIC PORTS ON MODEL C-134
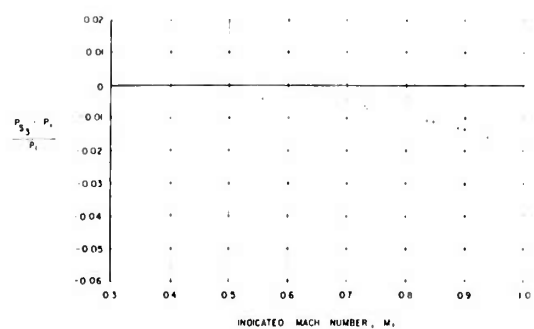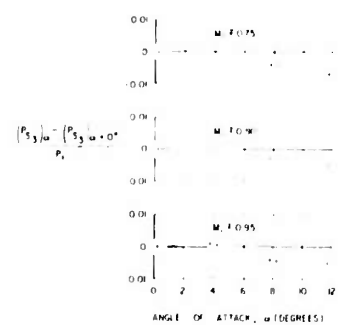
EXPERIMENTAL DATA (AEDC ONE FOOT TRANSONIC MODEL TUNNEL)

△,▽ EXPERIMENTAL DATA (AEDC E I SUPERSONIC TUNNEL)

FIGURE 30(A)
SUBSONIC PERFORMANCE OF S_2 AND S_3 PORTS ON
TEST MODELS C-38, C-39, C-98, AND C-134
$\alpha = 0°$

S_2 PORTS OF MODEL C-38 (AEDC ONE FOOT TRANSONIC MODEL TUNNEL)
S_2 PORTS OF MODEL C-39 (LANGLEY 8 FOOT TRANSONIC TUNNEL)
S_2 PORTS OF MODEL C-98 (AEDC ONE FOOT TRANSONIC MODEL TUNNEL)
S_3 PORTS OF MODEL C-98 (AEDC ONE FOOT TRANSONIC MODEL TUNNEL)
S_2 PORTS OF MODEL C-134 (AEDC ONE FOOT TRANSONIC MODEL TUNNEL)
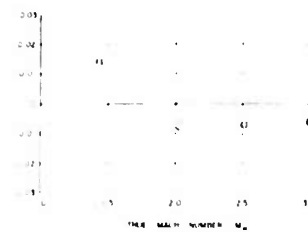
FIGURE 30(B)
SUPERSONIC PERFORMANCE OF S_2
PORTS ON MODEL C-134
$\alpha = 0°$

EXPERIMENTAL DATA AEDC E 1 SUPERSONIC TUNNEL
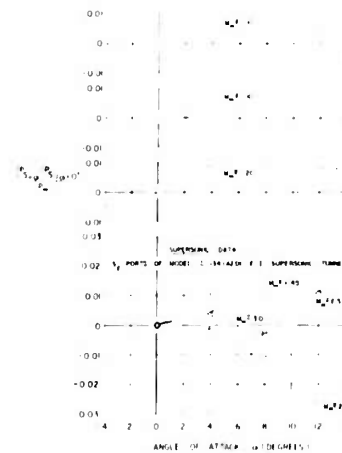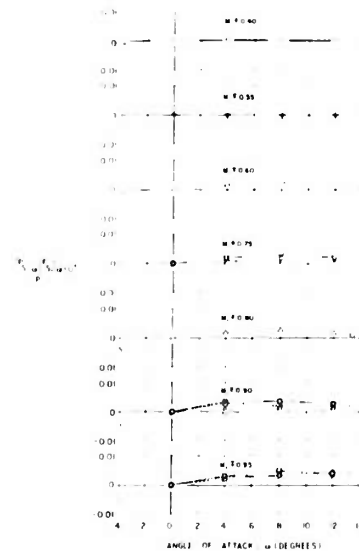
FIGURE 30(C)
ANGLE OF ATTACK PERFORMANCE OF S_2 AND S_3 STATIC PORTS
ON MODELS C-38, C-39, C-98, AND C-134
SUBSONIC AND TRANSONIC DATA
S_2 PORTS OF MODEL C-38 (AEDC ONE FOOT TRANSONIC MODEL TUNNEL)
S_2 PORTS OF MODEL C-39 (LANGLEY 8 FOOT TRANSONIC TUNNEL)
S_2 PORTS OF MODEL C-98 (AEDC ONE FOOT TRANSONIC MODEL TUNNEL)
S_3 PORTS OF MODEL C-98 (AEDC ONE FOOT TRANSONIC MODEL TUNNEL)
S_2 PORTS OF MODEL C-134 (AEDC ONE FOOT TRANSONIC MODEL TUNNEL)

-66-
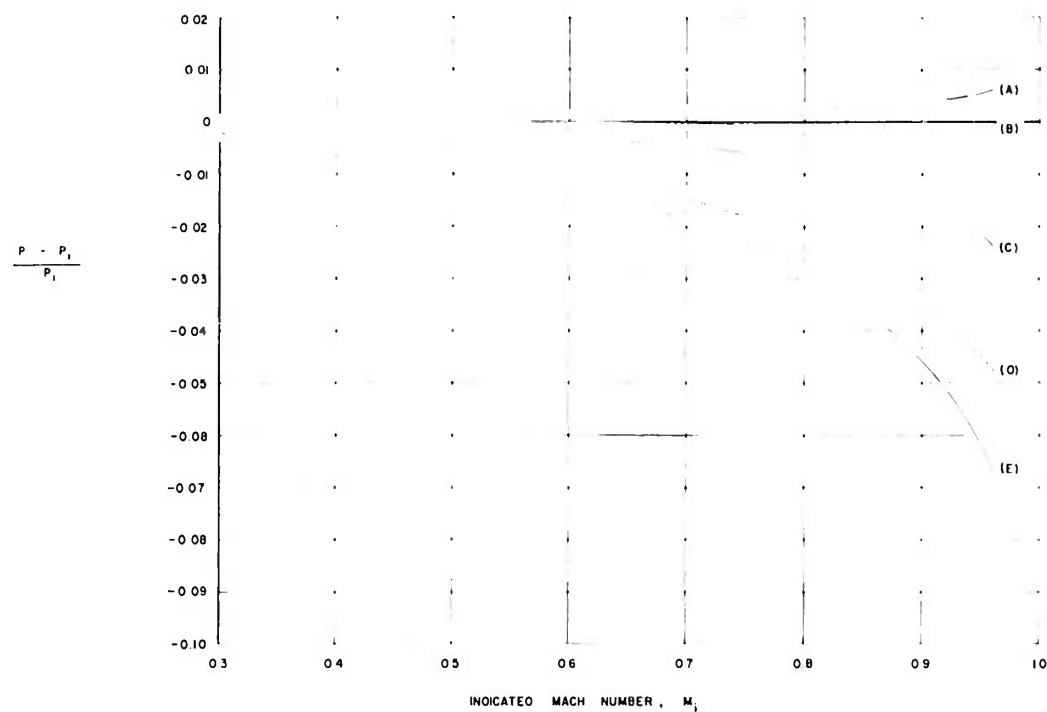
FIGURE 31

THEORETICAL   PREDICTION OF   COMPENSATION   OF

S_1/S_2 STATIC   PORTS

ON   MODELS   D-41,   D-123,   D-147,   AND   O-159.

$\alpha = 0°$

(A)   POSITIVE   PRESSURE   INDUCED   BY   REAR   ADAPTER   TAPERS

(B)   NEGATIVE   PRESSURE   INDUCED   BY   PITOT   OPENING

(C)   NEGATIVE   PRESSURE   INDUCED   BY   0.72°   FORWARD   TAPER

(D)   NEGATIVE   PRESSURE   INDUCED   BY   COMPENSATING   AFTERBODY   CONTOUR

(E)   TOTAL   COMPENSATION   OF S_1/S_2 STATIC   PORTS,

SUMMATION   OF   CURVES   (A), (B), (C),   AND   (D)

-67-
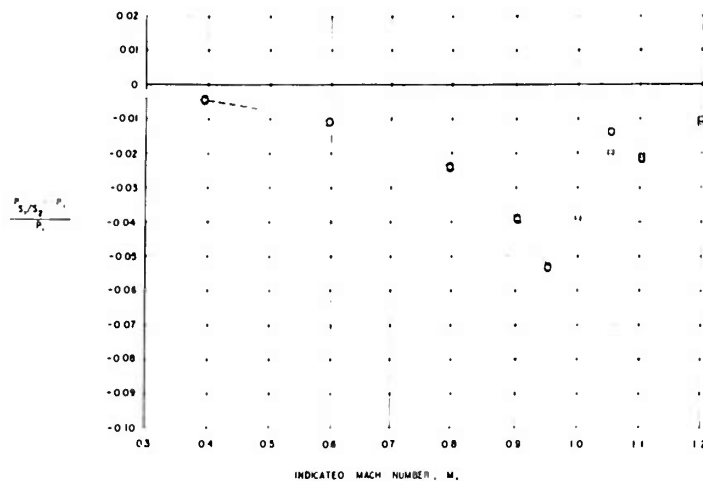
FIGURE 32(A)

SUBSONIC PERFORMANCE OF S_1/S_2 STATIC PORTS ON MODEL D-40

$\alpha = 0°$

EXPERIMENTAL DATA (LANGLEY 8 FOOT TRANSONIC TUNNEL)

---- THEORETICAL PREDICTION
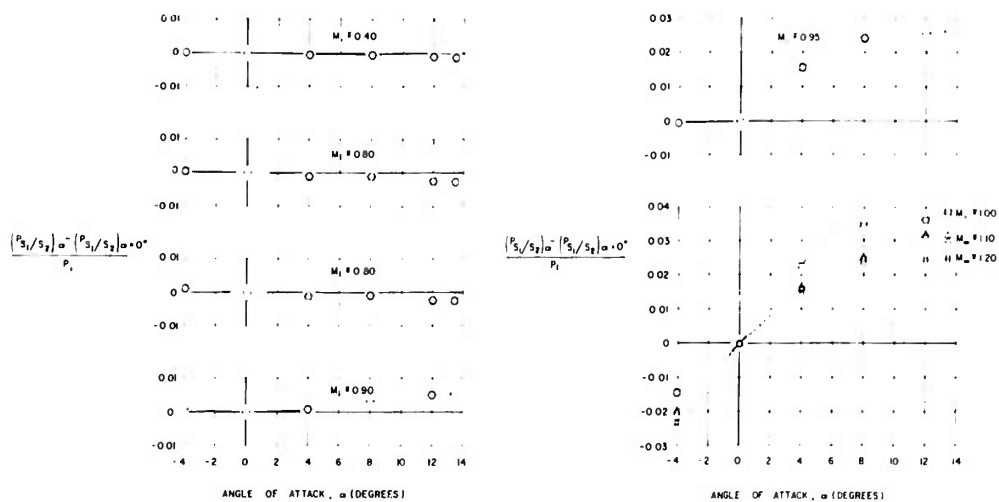
FIGURE 32(B)

ANGLE OF ATTACK PERFORMANCE OF S_1/S_2 STATIC PORTS ON MODEL D-40

(EXPERIMENTAL DATA - LANGLEY 8 FOOT TRANSONIC TUNNEL)

FIGURE 33(A)

SUBSONIC PERFORMANCE OF S_1/S_2 STATIC PORTS
ON MODEL D - 102

$\alpha = 0°$

EXPERIMENTAL DATA
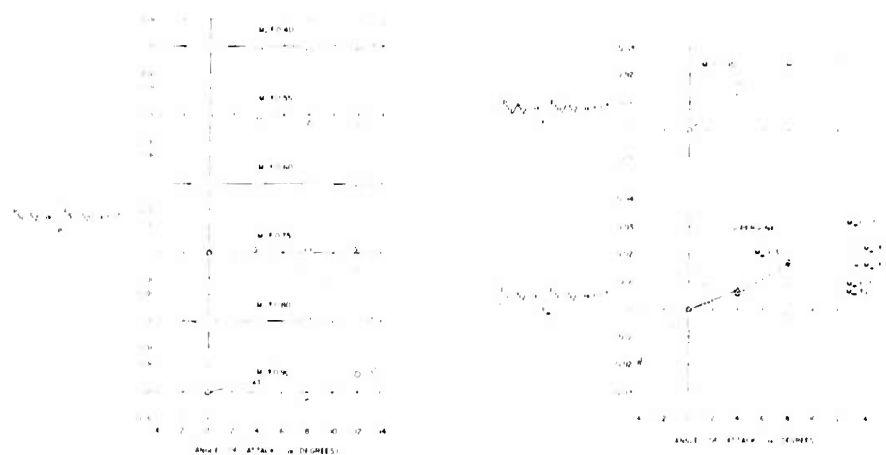(AEDC ONE FOOT TRANSONIC MODEL TUNNEL)
--- THEORETICAL PREDICTION

FIGURE 33(B)

ANGLE OF ATTACK PERFORMANCE
OF S_1/S_2 STATIC PORTS ON
MODEL D - 102

(EXPERIMENTAL DATA - AEDC ONE FOOT
TRANSONIC MODEL TUNNEL)

FIGURE 33(C)

SUBSONIC PERFORMANCE OF S_3 STATIC PORTS ON
MODEL D - 102

$\alpha = 0°$

EXPERIMENTAL DATA
(AEDC ONE FOOT TRANSONIC MODEL TUNNEL)

FIGURE 33(D)

ANGLE OF ATTACK PERFORMANCE
OF S_1 STATIC PORTS ON MODEL
D - 102

(EXPERIMENTAL DATA - AEDC ONE FOOT
TRANSONIC MODEL TUNNEL)
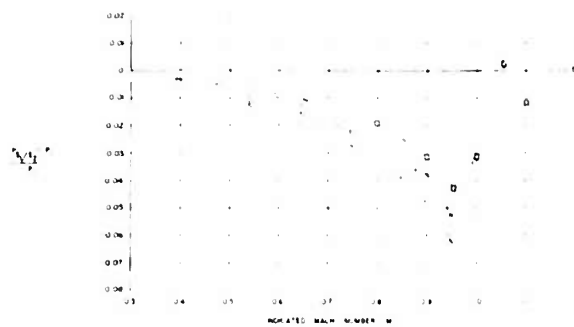
FIGURE 34(A)

SUBSONIC PERFORMANCE OF S_1/S_2 STATIC PORTS ON MODELS
D-41, D-123, AND D-147

α = 0°

EXPERIMENTAL DATA
    MODEL D-41 (LANGLEY 8-FOOT TRANSONIC TUNNEL)
    MODEL D-41 (AEDC ONE-FOOT TRANSONIC MODEL TUNNEL)
    MODEL D-123 (AEDC ONE-FOOT TRANSONIC MODEL TUNNEL)
    MODEL D-147 (AEDC ONE-FOOT TRANSONIC MODEL TUNNEL)

THEORETICAL PREDICTION
STATIC PRESSURE ERROR AT X = 1.25 INCHES AHEAD OF
EB TO, $P_m = P-1/P$
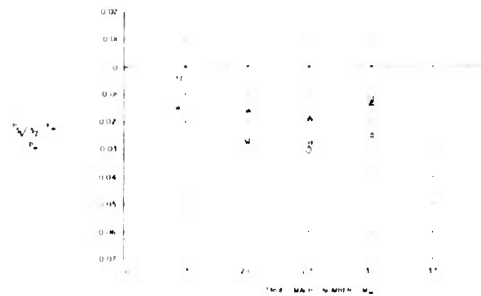
FIGURE 34(B)

SUPERSONIC PERFORMANCE OF S_1/S_2 STATIC PORTS ON MODELS
D-123, D-147, AND D-159

α = 0°

EXPERIMENTAL DATA
    MODEL D-123 (AEDC 1-2 SUPERSONIC WIND TUNNEL)
    MODEL D-147 (AEDC 1-2 SUPERSONIC WIND TUNNEL)
    MODEL D-159 (AEDC 1-2 SUPERSONIC WIND TUNNEL)

FIGURE 34(C)

ANGLE OF ATTACK PERFORMANCE OF S_1/S_2 STATIC PORTS ON MODELS D-41 AND D-123

EXPERIMENTAL DATA
    MODEL D-41 (LANGLEY 8-FOOT TRANSONIC TUNNEL)
    MODEL D-41 (AEDC ONE-FOOT TRANSONIC MODEL TUNNEL)
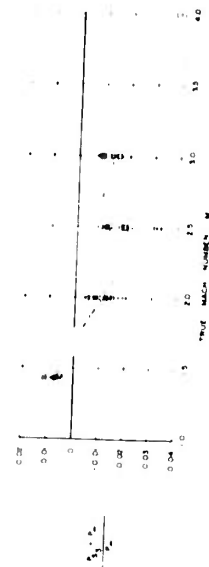   MODEL D-123 (AEDC ONE-FOOT TRANSONIC MODEL TUNNEL)
    MODEL D-123 (AEDC 1-2 SUPERSONIC TUNNEL)

-70-

FIGURE 34(E)

SUPERSONIC PERFORMANCE OF S_3 STATIC
PORTS ON MODELS 0-123, 0-147 AND 0-159
$\alpha = 0°$

EXPERIMENTAL DATA AEDC ( ): SUPERSONIC WIND TUNNEL
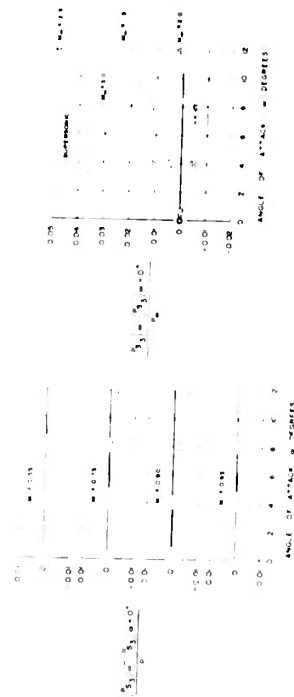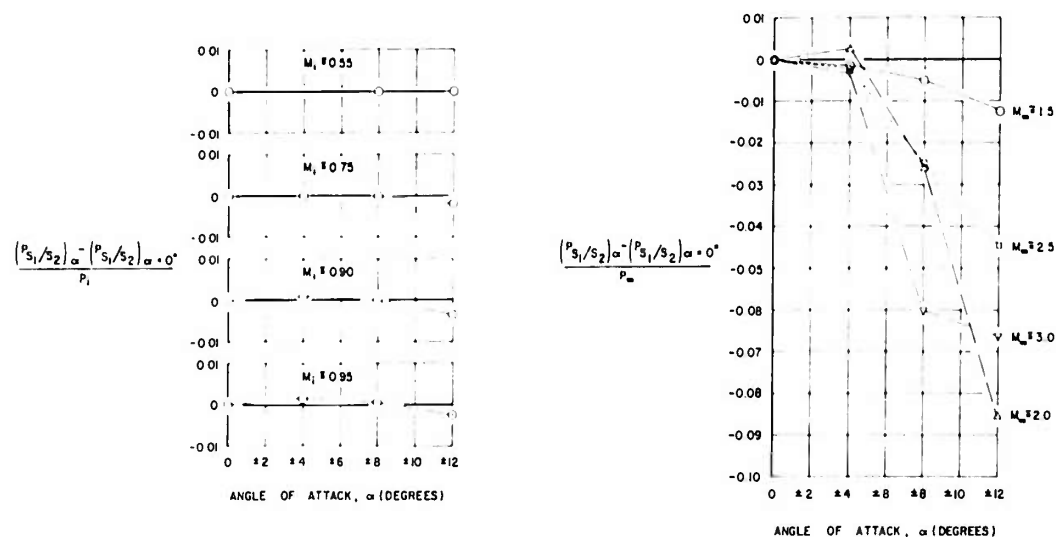△ MODEL 0-123
□ MODEL 0-147
○ MODEL 0-159

FIGURE 34(F)

ANGLE OF ATTACK PERFORMANCE OF S_3 STATIC PORTS
ON MODEL 0-123

EXPERIMENTAL DATA
SUBSONIC AEDC ONE FOOT TRANSONIC MODEL TUNNEL
SUPERSONIC AEDC ( ): ULTRASONIC TUNNEL

FIGURE 34(D)

SUBSONIC PERFORMANCE OF S_3 STATIC PORTS
ON MODELS 0-123 AND 0-147
$\alpha = 0°$

EXPERIMENTAL DATA AEDC ONE FOOT TRANSONIC MODEL TUNNEL
△ MODEL 0-123
○ MODEL 0-147

-71-

FIGURE 35(A)

ANGLE OF ATTACK PERFORMANCE OF S_1/S_2 STATIC PORTS ON MODEL D-147.

EXPERIMENTAL DATA

SUBSONIC (AEDC ONE FOOT TRANSONIC MODEL TUNNEL)
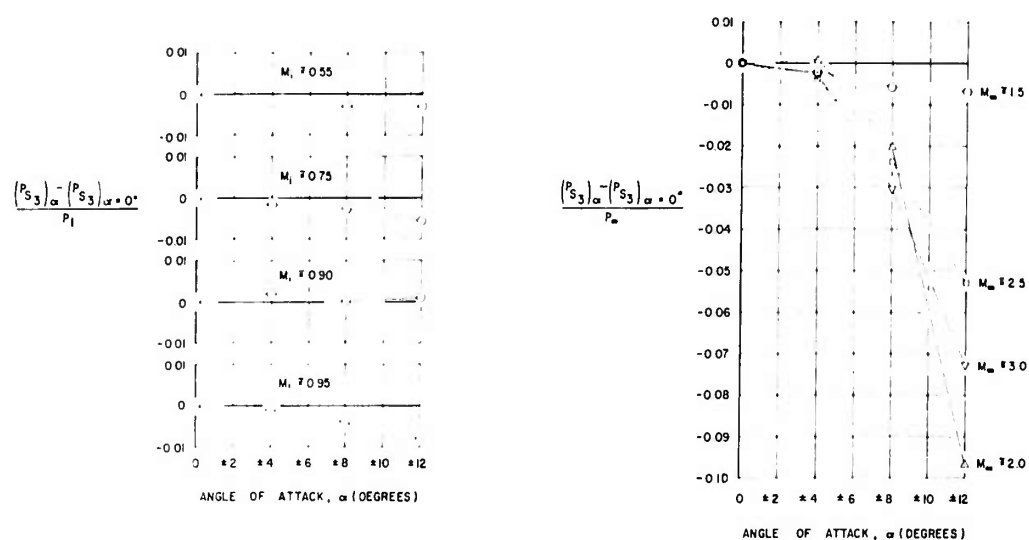SUPERSONIC (AEDC E-1 SUPERSONIC TUNNEL)

FIGURE 35(B)

ANGLE OF ATTACK PERFORMANCE OF S_3 STATIC PORTS ON MODEL D-147.

EXPERIMENTAL DATA

SUBSONIC (AEDC ONE FOOT TRANSONIC MODEL TUNNEL)
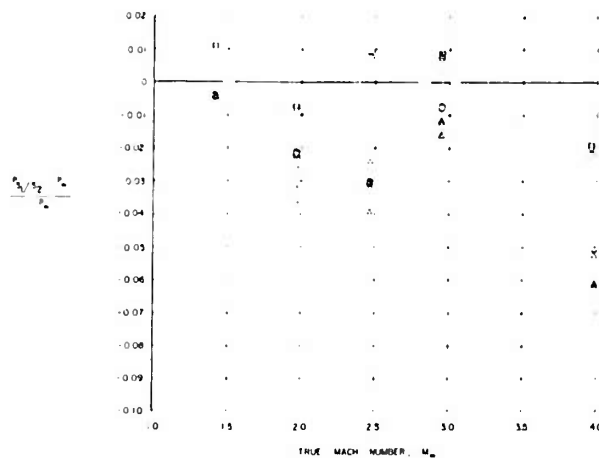SUPERSONIC (AEDC E-1 SUPERSONIC TUNNEL)

FIGURE 36(A)

SUPERSONIC PERFORMANCE OF S_1/S_2 STATIC PORTS ON

MODELS O-158 AND O-159

$\alpha = 0°$

EXPERIMENTAL RESULTS (AEDC E-I SUPERSONIC WIND TUNNEL)
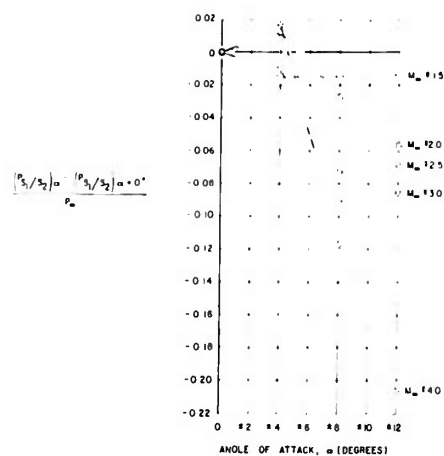
˅ MODEL O-158

△ MODEL O-159

FIGURE 36(B)

ANGLE OF ATTACK PERFORMANCE

OF S_1/S_2 PORTS ON MODEL O-158
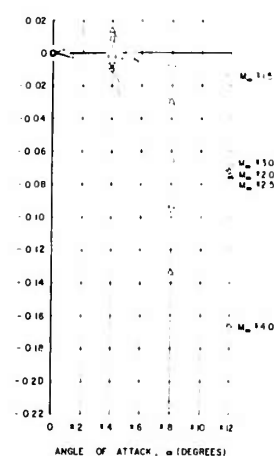
EXPERIMENTAL DATA

(AEDC E-I SUPERSONIC WIND TUNNEL)

FIGURE 36(C)

ANGLE OF ATTACK PERFORMANCE

OF S_1/S_2 PORTS ON MODEL O-159

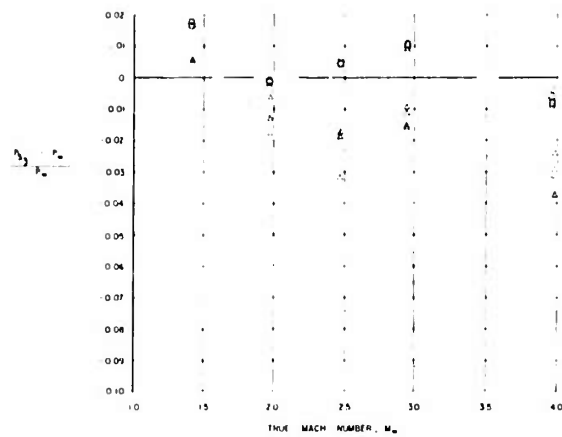EXPERIMENTAL DATA

(AEDC E-I SUPERSONIC WIND TUNNEL)

-73-

FIGURE 37(A)

SUPERSONIC PERFORMANCE OF S_3 STATIC PORTS ON
MODELS D-158 AND D-159
$\alpha = 0°$

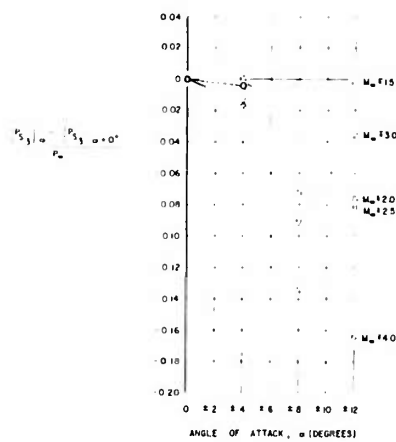EXPERIMENTAL DATA (AEDC E) SUPERSONIC WIND TUNNEL)
MODEL 0-158
△ MODEL 0-159

FIGURE 37(B)
ANGLE OF ATTACK PERFORMANCE
OF S_3 PORTS ON MODEL 0-158
EXPERIMENTAL DATA
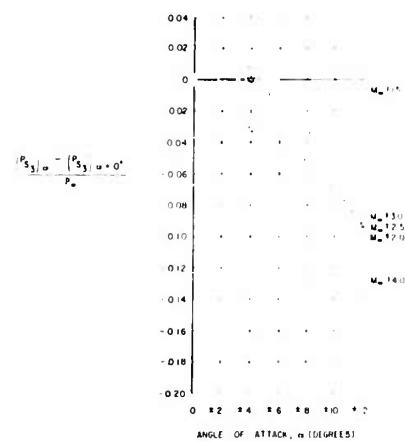(AEDC E-) SUPERSONIC WIND TUNNEL)

FIGURE 37(C)
ANGLE OF ATTACK PERFORMANCE
OF S_3 PORTS ON MODEL 0-159
EXPERIMENTAL DATA
(AEDC E) SUPERSONIC WIND TUNNEL)

-74-